Atmos. Chem. Phys. Discuss., 15, 3327–3379, 2015
www.atmos-chem-phys-discuss.net/15/3327/2015/
doi:10.5194/acpd-15-3327-2015

Atmospheric Chemistry and Physics Discussions

Low hygroscopic scattering enhancement of boreal aerosol and the implications for a columnar optical closure study

P. Zieger[1], P. P. Aalto[2], V. Aaltonen[3], M. Äijälä[2], J. Backman[2], J. Hong[2], M. Komppula[4], R. Krejci[1], M. Laborde[5,6], J. Lampilahti[2], G. de Leeuw[2,3], A. Pfüller[4], B. Rosati[7], M. Tesche[1], P. Tunved[1], R. Väänänen[2], and T. Petäjä[2]

[1]Department of Environmental Science and Analytical Chemistry & Bolin Centre for Climate Research, Stockholm University, Stockholm, Sweden
[2]Department of Physics, University of Helsinki, Helsinki, Finland
[3]Finnish Meteorological Institute, Climate Research Unit, Helsinki, Finland
[4]Finnish Meteorological Institute, Atmospheric Research Centre of Eastern Finland, Kuopio, Finland
[5]AerosolConsultingML GmbH, Lausanne, Switzerland
[6]Ecotech Pty Ltd., Melbourne, Australia
[7]Paul Scherrer Institute, Laboratory of Atmospheric Chemistry, Villigen, Switzerland

Received: 20 December 2014 – Accepted: 16 January 2015 – Published: 5 February 2015

Correspondence to: P. Zieger (paul.zieger@aces.su.se)

Published by Copernicus Publications on behalf of the European Geosciences Union.

ACPD
15, 3327–3379, 2015

Abstract

Ambient aerosol particles can take up water and thus change their optical properties depending on the hygroscopicity and the relative humidity (RH) of the surrounding air. Knowledge of the hygroscopicity effect is of crucial importance for radiative forcing calculations and is also needed for the comparison or validation of remote sensing or model results with in-situ measurements. Specifically, particle light scattering depends on RH and can be described by the scattering enhancement factor $f(\mathrm{RH})$, which is defined as the particle light scattering coefficient at defined RH divided by its dry value (RH < 30–40 %).

Here, we present results of an intensive field campaign carried out in summer 2013 at the SMEAR II station at Hyytiälä, Finland. Ground-based and airborne measurements of aerosol optical, chemical and microphysical properties were conducted. The $f(\mathrm{RH})$ measured at ground by a humidified nephelometer is found to be significantly lower (1.53 ± 0.24 at RH = 85 % and λ = 450 nm) than observed at other European sites. One reason is the high organic mass fraction of the aerosol encountered at Hyytiälä to which $f(\mathrm{RH})$ is clearly anti-correlated ($R^2 \approx 0.8$). A trajectory analysis revealed that elevated values of $f(\mathrm{RH})$ and the corresponding elevated inorganic mass fraction are partially caused by transported hygroscopic sea spray particles. An optical closure study shows the consistency of the ground based in-situ measurements.

Our measurements allow to determine the ambient particle light extinction coefficient using the measured $f(\mathrm{RH})$. By combining the ground-based measurements with intensive aircraft measurements of the particle number size distribution and ambient RH, columnar values of the particle extinction coefficient are determined and compared to direct measurements of a co-located AERONET Sun photometer. The water uptake is found to be of minor importance for the column averaged properties due to the low particle hygroscopicity and the low RH during the daytime of the summer months. The in-situ derived aerosol optical depth (AOD) clearly correlates with directly measured values ($R^2 \approx 0.9$ for λ = 400 nm to $R^2 \approx 0.6$ for λ, = 1000 nm), but is significantly lower

ACPD
15, 3327–3379, 2015

compared to the Sun photometer AOD (slope ≈0.5). The comparison degrades for longer wavelengths. The disagreement between in-situ derived and directly measured AOD is hypothesized to originate from losses of coarse and fine mode particles through dry deposition within the canopy and losses in the in-situ sampling lines. In addition, elevated aerosol layers (above 3 km) from long-range transport were observed using an aerosol lidar at Kuopio, Finland, about 200 km east-northeast of Hyytiälä. These elevated layers further explain parts of the disagreement.

1 Introduction

The uptake of water by atmospheric aerosol particles depends on the particle's hygroscopicity and the ambient relative humidity (RH). The exchange of water vapour with the environment causes a change in size and refractive index of aerosol particles, and therefore directly influences its optical properties. Especially the particle light scattering coefficient σ_{sp} is strongly dependent on RH. The main quantity describing this effect is called the scattering enhancement factor $f(\mathrm{RH},\lambda)$ which is defined as $\sigma_{sp}(\lambda)$ at elevated RH divided by its dry value

$$f(\mathrm{RH},\lambda) = \frac{\sigma_{sp}(\mathrm{RH},\lambda)}{\sigma_{sp}(\mathrm{RH_{dry}},\lambda)}, \quad (1)$$

where λ denotes the wavelength, which will be omitted from now on for simplicity. Nevertheless, one should keep in mind that all optical properties are dependent on λ.

Long-term in-situ measurements of aerosol scattering coefficients are usually performed at dry conditions (WMO/GAW, 2003, for example, recommends a RH below 30–40 %), but these in situ measured values differ from the ambient and thus climate relevant ones. Knowledge of this RH-effect is therefore important for the calculation of the direct aerosol radiative forcing (see e.g. Pilinis et al., 1995). In addition, the RH-effect is also important for the validation of model parameterizations (Zieger et al., 2013) or for the comparison and validation of remote sensing to in-situ measurements

ACPD
15, 3327–3379, 2015

(e.g., Tesche et al., 2014; Zieger et al., 2011, 2012; Esteve et al., 2012; Morgan et al., 2010; Voss et al., 2001; Ferrare et al., 1998).

The magnitude of f(RH) mainly depends on the aerosol chemical composition and size. Several studies have experimentally determined f(RH) for different ambient aerosol types using humidified nephelometer systems (see e.g. Fierz-Schmidhauser et al., 2010c; Covert et al., 1972; Pilat and Charlson, 1966, and Sect. 3.1). Arctic and marine aerosols usually show the greatest values of f(RH) which decrease with increasing anthropogenic influence (e.g. f(85 %, 550 nm) ≈ 2–3.5; Titos et al., 2014a; Zieger et al., 2010; Fierz-Schmidhauser et al., 2010b; Wang et al., 2007; Carrico et al., 1998, 2000, 2003; Gasso et al., 2000; McInnes et al., 1998). Continental aerosols (e.g. f(85 %, 550 nm) ≈ 1.8–2.8; Zieger et al., 2012, 2014; Fierz-Schmidhauser et al., 2010a; Koloutsou-Vakakis et al., 2001; Sheridan et al., 2001) and urban aerosols (e.g. f(85 %, 550 nm) ≈ 1.3–1.6; Titos et al., 2014b; Zieger et al., 2011; Yan et al., 2009; McInnes et al., 1998; Fitzgerald et al., 1982) are observed with intermediate values. Low values are usually seen for biomass burning aerosol (e.g. f(80 %, 550 nm) ≈ 1.0.1–1.51; Kotchenruther and Hobbs, 1998) or for highly polluted air masses (e.g. f(80 %, 550 nm) ≈ 1.07–2.35; Pan et al., 2009). Low values have also been reported for mineral dust which can be transported over long distances e.g. from the Sahara to the European continent (e.g. f(85 %, 550 nm) ≈ 1.2–1.7; Titos et al., 2014b; Zieger et al., 2012; Fierz-Schmidhauser et al., 2010a). In boreal environments, the aerosol particles are typically less hygroscopic (Swietlicki et al., 2008; Ehn et al., 2007; Petäjä et al., 2005; Hämeri et al., 2001) due to a large contribution of organics (Allan et al., 2006). So far, the f(RH) of particles representative for boreal regions has not been characterized in great detail. This is the topic of the current study where f(RH) is analyzed combining highly time resolved, and detailed aerosol microphysical and chemical measurements. The results are further used to extrapolate the ground-based in-situ measurements, which includes the RH-effect on the particle light scattering, to the atmospheric column using airborne measurements of the particle number concentration and size.

ACPD
15, 3327–3379, 2015

The motivation for this study is based on two research questions:

1. What is the magnitude of the scattering enhancement factor $f(\mathrm{RH})$ in the boreal forest region of northern Europe?

2. Can an optical closure between ground-based in-situ and remote sensing aerosol measurements be achieved?

2 The field site at Hyytiälä

A measurement campaign with ground-based and airborne measurements was carried out from May 2013 to August 2013 at the SMEAR II station at Hyytiälä, Finland, as part of the EU-FP7 project PEGASOS (Pan-European Gas-Aerosols-climate interaction Study). The station is located in southern Finland (61.85° N, 24.28° E, 180 m a.s.l.) and is surrounded by a dense coniferous forest and several lakes. The largest city close by is Tampere (60 km south-west of the site). More details on the long-term in-situ measurements and the site can be found in Vesala et al. (1998) and Hari and Kulmala (2005). Most of the instrumentation used for monitoring purposes of aerosol properties was located in separate cottages within the forest, while the instruments installed specifically for the PEGASOS campaign were located in separate measurement containers and had their own inlets (see Sect. 3). The containers were located on an open parking lot 30 m away from the main cottage, where most of the aerosol monitoring instruments were located.

In May and June 2013, intensive airborne measurements were conducted around Hyytiälä. This included sampling from an airship (Zeppelin) and more frequently from a Cessna (see Sect. 3.6), which data will be used in this study. The ground-based in-situ measurements continued until the beginning of August 2013.

ACPD
15, 3327–3379, 2015

3 Instrumental

3.1 Particle hygroscopicity measurements

A humidified nephelometer (WetNeph) was deployed to measure the effect of water uptake on the particle light scattering coefficient. The instrument is described in detail by Fierz-Schmidhauser et al. (2010c); hence, a brief description will be given here. The WetNeph consists of a specifically designed single-stream humidification system, where the aerosol first enters a humidifier (at a flow rate of 9.5 lpm) and then a drier before the particle light-scattering coefficients are measured by an integrating nephelometer at three wavelengths (λ = 450, 525, 635 nm). A LED based nephelometer (Ecotech Pty Ltd., Aurora 3000) was used, which is less affected by the heat of the lamp that could influence the RH inside the nephelometer. The WetNeph was set to the humidograph mode, where the RH inside the nephelometer is periodically cycled between 35–40 % and 90–95 % (slightly depending on the temperature inside the measurement container). This set-up allows to measure the upper and lower branch of the aerosol hysteresis curve separately. Dry scattering coefficients were measured in parallel with a second (reference) nephelometer of the same type as the WetNeph with an average RH inside the nephelometer cell of 6.5 ± 3.5 % (mean ± standard deviation; SD). From this data, Eq. (1) is then used to calculate f(RH) for each nephelometer wavelength.

All scattering coefficients were corrected for the truncation error and non-idealities of the light source by the scheme described in Müller et al. (2011). First, the nephelometers were calibrated using particle free air and CO_2 as a span gas. Then, both nephelometers were run in parallel, measuring the same aerosol at the same RH, to determine the relative differences between the two instruments. Relative differences between 5 and 12 % were found for the three wavelengths, which was accounted for when calculating the intensive parameter f(RH). In addition, measured humidograms of polydisperse ammonium sulphate particles were compared to model predictions (Fierz-Schmidhauser et al., 2010c) using the size distributions measured by a DMPS system

ACPD
15, 3327–3379, 2015

(with a diameter range of 6 to 600 nm, see below), theoretical growth factors of ammonium sulphate and Mie theory. Good agreement was found, however the modelled values of f(RH) were 5–10 % above the measured values, which can be attributed to firstly the presence of few large particles that were not included in the model calculations (due to the size cut of the DMPS) and would lead to a lower predicted f(RH) (Zieger et al., 2013), and secondly to the RH sensor's uncertainty (1–2 % absolute difference, Rotronic HygroClip) and finally to the losses in the WetNeph system itself (between 2.5–5 %, Fierz-Schmidhauser et al., 2010c). The WetNeph has also been successfully compared to a novel commercially available humidified nephelometer system (aerosol conditioning system (ACS1000) by Ecotech Pty Ltd.).

The humidograms of f(RH) can be described by an empirical two parameter fit (e.g., Clarke et al., 2002; Carrico et al., 2003):

$$f(\mathrm{RH}) = a(1 - \mathrm{RH})^{-\gamma}. \quad (2)$$

The parameter a in Eq. (2) is the intercept at RH = 0 % while γ describes the magnitude of the measured f(RH). In previous work (Zieger et al., 2011, 2014), the upper and lower branches were fitted separately to the humidograms to investigate the existence of aerosol deliquescence (sudden transition from the solid to the liquid state of the particles; usually caused by pure inorganic salts). However, no deliquescence was observed at Hyytiälä due to the dominance of organic substances.

While f(RH) represents the hygroscopic growth as an optical measure, one can also describe the hygroscopic growth by the change in particle diameter. The hygroscopic growth factor g(RH) is defined as the ratio of the particle diameter at elevated RH to its dry diameter

$$g(\mathrm{RH}) = \frac{D_{\mathrm{p,wet}}(\mathrm{RH})}{D_{\mathrm{p,dry}}}. \quad (3)$$

g(RH) was determined using a hygroscopicity tandem differential mobility analyzer (H-TDMA), which is part of a volatile hygroscopicity tandem differential mobility analyzer (VH-TDMA) system. Detailed information on the system can be found in Hong

ACPD
15, 3327–3379, 2015

et al. (2014). Four dry mobility diameters were selected ($D_{p,dry}$ = 30, 60, 100, 145 nm) and their humidified size distribution was measured at RH = 90±2 % by a second differential mobility analyzer (DMA) and condensation particle counter (CPC, TSI Inc, Model 3772) system. The H-TDMA was calibrated with ammonium sulphate particles at 90 % RH before the ambient sampling.

3.2 Particle absorption measurements

A filter based absorption photometer (aethalometer, Model AE-31, Maggee Scientific) was used to measure equivalent black carbon (EBC) mass concentrations (Weingartner et al., 2003; Petzold et al., 2013). The aethalometer is a multi-wavelength instrument that measures the particle light absorption coefficient σ_{ap} at seven wavelengths by recording the attenuation of light through a filter where particles deposit. The instrument then converts the subsequent increase in attenuation to EBC concentrations using a mass absorption cross section of 14 625 nm m^2 g^{-1} λ^{-1}. The instrument was measuring behind a Digitel PM_{10} ambient humidity inlet with a flow rate of 30 lpm. A site-specific correction factor of $C = 3.35$ to correct for multiple scattering within the filter was applied (Weingartner et al., 2003). A more detailed description of the aethalometer measurements at the site is given by Virkkula et al. (2011).

3.3 Particle size distribution measurements

The particle number size distribution was determined at ground level using a differential mobility particle sizer (DMPS) for the fine mode (electrical mobility diameter, $D_p < 1$ µm) and an aerodynamic particle sizer (APS) for the coarse mode (aerodynamic particle diameter $D_p > 1$ µm). The Hyytiälä-DMPS is a twin DMPS set-up. DMPS1 has a 10.9 cm long Vienna type DMA followed by a CPC (TSI Inc., Model 3025). The measurement range is 3 to 40 nm (electrical mobility diameter) with a sheath flow rate of 20 lpm and an aerosol flow rate of 4 lpm. DMPS2 has a 28 cm long Vienna type DMA, followed by a CPC (TSI Inc., Model 3772). The measurement range of DMPS2 is between 20 to

ACPD
15, 3327–3379, 2015

1000 nm with a sheath air of 5 lpm and an aerosol flow rate of 1 lpm. The sheath flows of the twin DMPS are dried to RH < 40 %, and continuously controlled with regulating valves and in-line flow meters. The aerosol flow is brought to charge balance using a ^{14}C radioactive source and the flows are monitored using pressure drop flow meters. One measurement cycle takes about 10 min. The Hyytiälä-DMPS is regularly calibrated and checked with standard polystyrene latex spheres particles, higher precision flow meters and has also been successfully intercompared to the ACTRIS moving standard in 2009 (Wiedensohler et al., 2012). In addition to the twin DMPS, the APS (TSI Inc., Model 3321) measured the size distribution in the aerodynamic diameter range between 520 nm and 20 µm. The aerosol is aspirated through a straight sampling line (tube diameter 16 mm, length 4 m) to the instrument to avoid particle losses. The inlet is at a height of 6 m above the ground and consists of a total suspended particle inlet (Digitel Inc.). The inlet is heated to 40 °C to prevent condensation, to ensure that fog droplets are evaporated and that the RH is below 40 %.

3.4 Particle chemical composition measurements

The aerosol chemical composition was measured by an aerosol chemical speciation monitor (ACSM, Aerodyne Research ltd.) which is permanently deployed at Hyytiälä since March 2012. The instrument is a lighter version of the Aerodyne aerosol mass spectrometer (Canagaratna et al., 2007) developed for monitoring purposes. The measured mass is assigned to five main chemical species: sulphates (SO_4), nitrates (NO_3), ammonia (NH_4), chlorides (Cl) and organics (Org). For a more detailed description on the data processing, the reader is referred to the studies by Allan et al. (2003, 2004), while more technical details on the ACSM can be found in Ng et al. (2011).

Assuming internally and externally well-mixed aerosol, the molar concentrations of inorganic ions can be assigned to typically observed inorganic salts: ammonium sulphate ($(NH_4)_2SO_4$), ammonium bisulphate ($(NH_4)HSO_4$), and ammonium nitrate (NH_4NO_3). Since the amount of chlorides at Hyytiälä was negligibly low, ammonium chloride (NH_4Cl) was excluded from the calculations. It was assumed that ammonium

ACPD
15, 3327–3379, 2015

ions first pair with SO_4-ions to form ammonium sulphate and/or bisulphate – depending on the molar ratio of NH_4 to SO_4 – with the remaining amount of NH_4 being available to form ammonium nitrate. Leftover NO_3 was considered to originate from organic nitrates. The loadings of NH_4 were typically too low to fully neutralize all of the observed SO_4 and NO_3. Occasionally, the SO_4 was left un-neutralized, in which case they were considered to originate from sulfuric acid (H_2SO_4). It should be noted that the above calculations are very sensitive to the assumption of well-mixed aerosol, and additionally fail to account for possible organic salts (e.g. organonitrate and organosulphate compounds). As these assumptions are extreme in an ambient aerosol situation, the estimate must be considered only a rough first approximation. However, it does provide some quantitative results which we can use to predict f(RH), as shown in Sect. 6.1.

Submicron elemental carbon (EC) mass concentration was measured using a semi-continuous OC/EC analyzer (Sunset Technologies Inc). The instrument measures the mass concentrations of organic carbon (OC) and EC with a time-resolution of approximately three hours. The device utilized a two-step thermal-optical method for the determination of OC and EC. More details can be found in Peterson and Richards (2002) and Karanasiou et al. (2011).

The chemical mass fraction was determined by dividing the individual components of the ACSM and EC/OC analysis by the sum of all (excluding the OC from the EC/OC analysis, which is covered by the ACSM measurement). The organic mass fraction was determined by adding the EC part (which is known to have a low hygroscopicity) of the EC/OC analysis to the organic components of the ACSM. The mass fraction is representative for sub-micron particles only due to the experimental restrictions.

3.5 Auxiliary in-situ instruments

Within the monitoring network, an integrating nephelometer (TSI Inc., Model 3563) is used to measure $\sigma_{sp,\,dry}$ at λ = 450, 550, and 700 nm. The instrument is located in the aerosol cottage behind an switching PM_1 and PM_{10} inlet. Here, only the PM_{10} mea-

ACPD
15, 3327–3379, 2015

surements of $\sigma_{sp,\,dry}$ are used to retrieve the complex refractive index and to compare the measurements of the WetNeph reference nephelometer to it.

Meteorological parameters like temperature, wind speed and direction or RH were continuously measured along a 124 m high tower.

3.6 Airborne measurements

Vertical profiles of the aerosol size distributions were measured using a Cessna 172 F aircraft as a platform (Schobesberger et al., 2013; Leino et al., 2014). The total particle concentration was measured using an ultrafine condensation particle counter (uCPC, TSI Inc, Model 3776) with a diameter cut off size of 3 nm. A scanning mobility particle sizer (SMPS, Wang and Flagan, 1990) with a small Hauke type DMA and CPC (TSI Inc, TSI 3010) was used to determine the particle number size distribution (mobility diameter size range of 10–270 nm). For the SMPS the inversion by Collins et al. (2002) was used, and the calibration corrections and turbulent tube losses were taken into account. Other instruments inside the cabin included the Li-Cor 840 gas analyzer measuring H_2O and CO_2 concentrations and a pressure sensor. Ambient air temperature was measured using a PT100 sensor. A GPS receiver recorded the flight path. The sample air inlet was a down-scaled version of the inlet design used with University of Hawaii's DC-8 (McNaughton et al., 2007). It was situated under the right wing out from the propeller flow. The sample air was led inside the aircraft via a stainless steel tube of length 4.2 m and diameter of 22 mm. The flow rate of the inlet tube was between 45–50 lpm.

The flights were conducted with a slow airspeed of $\approx 130\,km\,h^{-1}$. The ascend or descent rate was around $2.5\,m\,s^{-1}$. Most of the research flights (23/30) were conducted above the area surrounding the SMEAR II station at Hyytiälä. The other flights were performed around Jämijärvi airport located 80 km west of Hyytiälä. The flight profiles usually contained several flight paths of around 30 km with constant altitudes and additionally a climb up to 3.2 km. The direction of the flight paths was chosen to be per-

ACPD
15, 3327–3379, 2015

pendicular to the wind direction at ground. The measurements are described in more detail by Väänänen et al. (2015).

3.7 Columnar and vertical measurements of aerosol optical properties

Columnar aerosol optical properties were measured using a Sun photometer (CIMEL CE-318) which has been operated at Hyytiälä since February 2008 (Aaltonen et al., 2012). The instrument was installed on a 18 m high tower above the canopy of the forest surrounding the station and is part of the AERONET network (Holben et al., 1998). It measures direct sun irradiance to obtain the aerosol optical depth (AOD) at different wavelengths (λ = 340, 380, 440, 500, 675, 870, 1020 and 1640 nm) and the Ångström exponent (see Eq. 6 below). Moreover, other optical and microphysical properties of atmospheric aerosols are routinely retrieved using an inversion scheme developed by Dubovik et al. (2006). The calibration is carried out yearly by comparison with reference instruments, after which final corrections are made and the data are available as quality assured level 2.0 data. The level 2.0 data has been used in the following analysis.

In addition to the AERONET measurements, data from a seven-channel Raman lidar (Polly^{XT}; Althausen et al., 2009; Engelmann et al., 2012) was included in the data analysis. The lidar is located in Kuopio (62°44′17″ N, 27°32′33.5″ E, 190 m a.s.l.) which is 200 km east-northeast of Hyytiälä. It is operated by the Finnish Meteorological Institute (FMI) within the Finnish observation network (Hirsikko et al., 2014) and is part of the European Aerosol Research lidar Network (EARLINET). Polly^{XT} provides vertical profiles of particle backscatter coefficients at wavelengths of 355, 532 and 1064 nm, and the particle extinction coefficient at 355 and 532 nm. The system also includes a depolarization (532 nm) and a water-vapor (407 nm) channel. The vertical resolution of the instrument is 30 m.

ACPD
15, 3327–3379, 2015

4 Trajectory calculations

Air mass back trajectories were calculated hourly with the air parcel arriving at an altitude of 100 m above the site using the HYSPLIT model (Draxler, 2004; Draxler and Hess, 1998). The trajectories were calculated on the basis of the Global Data Assimilation System data set (GDAS, http://ready.arl.noaa.gov/archives.php). Along each trajectory, additional parameters such as mixing layer (ML) height, temperature, RH and column precipitation was calculated by the model. Each trajectory had a time length of 10 days.

The surface residence time of an air parcel was then calculated by adding the travel time of each trajectory for the entire measurement period on a $1^{\circ} \times 1^{\circ}$ longitudinal and latitudinal grid. Only periods when the air parcel was within the ML were considered.

To further differentiate between the continental and maritime influence the parameter ψ is introduced

$$\psi = \int_{t_{\text{start}}}^{t_{\text{end}}} (\rho(t) \cdot \epsilon(t))\,\mathrm{d}t, \tag{4}$$

where t_{start} denotes the start and t_{end} the arrival time of the trajectory. The factor $\epsilon(t)$ in Eq. (4) is +1 if the air parcel traverses within the ML above land, while it is −1 when the parcel traverses within the ML above oceans. The factor $\rho(t)$ accounts for the removal of the particles with an estimated half-lifetime of one week (assuming a quadratic decrease with time). Other removal mechanisms (e.g. due to precipitation) are not taken into account. By this definition, ψ has as outer boundaries −1 (air mass traversed only above oceans) and +1 (air mass traversed only above land). We are aware that this is a simplified way of classifying the air masses, however, it will be shown that ψ sufficiently describes the maritime and continental influence for our purposes.

ACPD
15, 3327–3379, 2015

5 Results

Section 5.1 describes the results of in-situ measurements of f(RH), its parametrization and correlation to the particle's chemical composition. The following Sect. 5.2 explains the extrapolation of the ground-based in-situ measurements to the atmospheric column and compares the result to routinely performed Sun photometer measurements. Different hypothesis are discussed in Sect. 6 that can impact the comparison.

5.1 Influence of water uptake on the aerosol light scattering coefficient at Hyytiälä

The time series of f(RH) at RH = 85 % was calculated by averaging the humidograms every three hours (one full RH cycle) and applying Eq. (2) to the measurements. The result is shown in Fig. 1 together with the corresponding dry scattering coefficient $\sigma_{\mathrm{sp,\,dry}}$ for λ = 525 nm. f(RH = 85 %, 525 nm) shows little variation throughout the summer months with a mean value of 1.63 ± 0.22. f(RH = 85 %, 525 nm) decreases with increasing dry scattering coefficient $\sigma_{\mathrm{sp,\,dry}}$, indicating an increased presence of less hygroscopic particles at high $\sigma_{\mathrm{sp,\,dry}}$. The probability density function (PDF) of the measured f(RH = 85 %) for all nephelometer wavelengths and the entire campaign is shown in Fig. 2 together with the PDF of the fit parameters used in Eq. (2). A small increase of f(RH = 85 %) with increasing wavelength is observed, similar to observations made at Melpitz, Germany (Zieger et al., 2014). This effect can be reproduced by calculating the optical properties using Mie theory with the input of the measured size distribution and chemical composition of the particles. The fit-parameter γ and a consequently show a low variation with a mean and SD value of 0.25 ± 0.07 and 1.01 ± 0.05, respectively. The value of $a \approx 1$ indicates the absence of hysteresis effects. The mean, SD and percentile values of f(RH = 85 %) are given for all wavelengths in Table 1 together with the fit parameters (see Eq. 2).

The f(RH) observed at Hyytiälä is remarkably low compared to other sites. Figure 3 shows the PDF at RH = 85 % and λ = 550 nm (linearly interpolated) in comparison to

ACPD
15, 3327–3379, 2015

other European sites (Zieger et al., 2013). High values of f(RH) were measured for pristine maritime and Arctic aerosol found at Ny-Ålesund, Spitsbergen (campaign mean and SD: f(85 %, 550 nm) = 3.24 ± 0.63), or aerosol dominated by inorganic salts as recorded in winter 2009 at Melpitz, Germany (f(85 %, 550 nm) = 2.77 ± 0.37). Intermediate values were usually measured for continental and anthropogenic influenced aerosol at Cabauw, the Netherlands (f(85 %, 550 nm) = 2.38 ± 0.38), or free tropospheric aerosol at Jungfraujoch, Switzerland (f(85 %, 550 nm) = 2.30 ± 0.33). Mace Head in Ireland showed a large variation in f(RH) depending on the wind sector if the air had a maritime origin or was influenced from anthropogenic emissions (f(85 %, 550 nm) = 2.08 ± 0.29).

The reason for the low f(RH) at Hyytiälä can be explained by the dominance of organic substances in the particle chemical composition, which leads to lower particle hygroscopicity. As an example, the f(85 %, 450 nm) is plotted as a function of the organic mass fraction in Fig. 4. The linear least squares regression shows a clear anti-correlation (squared Pearson's correlation coefficient: R^2 = 0.78) with a decrease in f(RH) with increasing organic mass contribution. The dominance of the organic mass fraction (mean ± SD: 0.7 ± 0.11) clearly determines the low values of f(RH) observed at Hyytiälä. For comparison, the values measured at Melpitz, Germany, are added to Fig. 4 (for more details see Zieger et al., 2014). The organic mass fraction at Melpitz of sub-micrometer particles was significantly lower than at Hyytiälä (mean ± SD: 0.23 ± 0.10). Although the f(RH)-values for Melpitz were measured at a different time of year (winter) and showed a higher variability (R^2 = 0.53), they almost line up linearly with the observations made at Hyytiälä. Due to measurement restrictions the total mass at Melpitz was only differentiated between black and organic carbon, while the total mass at Hyytiälä is determined from the elemental carbon of the EC/OC analysis (organic carbon is assumed to be included in the ACSM organic mass fraction).

The comparison of the fit parameter γ and the main chemical mass fractions is shown in Table 2. The inorganic mass fractions, mainly sulphate and ammonia, are clearly positively correlated with γ and f(RH), in contrast to the organic mass fraction

ACPD
15, 3327–3379, 2015

which is anti-correlated. This allows to use the continuous performed chemical composition measurements at Hyytiälä to predict f(RH) if no humidified nephelometer is operated. This can be done by taking the total organic or inorganic mass fraction as a proxy for f(RH) and using the linear regression parameters given in Table 2 to calculate γ for each wavelengths. f(RH) then follows by using Eq. (2) assuming an intercept of $a = 1$ (see Table 1). However, this is only valid for the summer months when the fine mode at Hyytiälä is clearly dominated by less hygroscopic organic substances. Verification during other seasons is needed to allow for generalization of these findings at this site. Additionally, they may not be valid during periods with substantially different coarse mode contribution which can have a potentially large impact on the total f(RH) (Zieger et al., 2013).

The trajectory analysis reveals further insights to the source of f(RH) as shown in Fig. 5. Figure 5a reveals that the main catchment area of the air arriving at Hyytiälä was Southern Finland, Russia, the Baltic Sea, parts of Scandinavia and continental Europe as well as the Atlantic and Arctic Ocean. The f(RH = 85 %, 450 nm), the organic mass fraction and the EBC concentration were separately averaged on a $1^\circ \times 1^\circ$ grid if the air parcel of the trajectory was within the ML for each grid point. It is hereby assumed that the property did not change along the trajectory. It can be seen in Fig. 5b that air masses with eastern and continental origin had generally a lower f(RH), while air masses traversing over oceans or originating from the Arctic were characterized with elevated values of f(RH), which can be explained by the contribution of hygroscopic sea spray particles transported to Hyytiälä. Figure 5c shows the organic mass fraction which is clearly elevated for continental air masses, while it decreased for air masses having a maritime origin. Note that the time series of f(RH) has interruptions (see Fig. 1) compared to the organic mass fraction, which explains the different spatial patterns in Fig. 5. Figure 5d shows the spatial distribution of the EBC as measured by the aethalometer. A strong source of EBC around St. Petersburg in Russia and generally elevated concentrations of air masses coming from the continent can be seen. No weighting or removal was considered for this analysis since mainly intensive pa-

ACPD
15, 3327–3379, 2015

rameters are shown. In addition, the analysis is also influenced by shadowing effects, if air masses from different origin are averaged on the same grid point to one mean value. This can be avoided by using the factor ψ introduced in Eq. (4), which reveals the potential maritime and continental influence. Figure 6 shows the average values of $f(\mathrm{RH} = 85\,\%, 450\,\mathrm{nm})$, the EBC concentration and the organic mass fraction vs. ψ. It can be seen that the scattering enhancement is generally higher for maritime air masses, while it clearly decreases with increasing continental influence. As an opposite trend, the organic mass fraction steadily increases with more continental influence. The EBC values are only slightly increased for the continental air masses, however not as significant as the organic mass fraction.

The measured scattering enhancement factors have been compared to further in-situ measured aerosol and meteorological parameters. No clear and significant dependency was found if compared to the single scattering albedo, the scattering Ångström exponent, aerosol size distribution parameters (mean surface and total number concentration), wind direction or wind speed.

5.2 Extrapolation to the atmospheric column using aircraft measurements

The in-situ measurements were extrapolated to the atmospheric column using regular airborne profile measurements that were performed during the second half of May until mid of June 2013. In total 18 profiles with collocated cloud-free AERONET measurements on the ground were available. The measurements were binned in 200 m wide height levels. The profile flights time took on average 2.5 h and included up to three full ascends and descends. The 18 selected vertical profiles of the total particle number concentration measured by the aircraft's CPC are shown in Fig. 7a. As expected, the particle concentration decreased with altitude. A comparison of the aircraft measurement at the lowest flight level (200–400 m) to the ground-based CPC shows a good agreement ($R^2 = 0.80$, linear regression: $N_{\mathrm{tot}}^{\mathrm{Cessna}} = 1.17 N_{\mathrm{tot}}^{\mathrm{ground}} - 142\,\mathrm{cm}^{-3}$) and slightly less particles by the ground CPC (see Fig. 7b).

ACPD
15, 3327–3379, 2015

The AOD is defined as the vertical integral of the particle light extinction coefficient σ_{ep}

$$\mathrm{AOD}(\lambda) = \int_{h_0}^{h_1} \sigma_{\mathrm{ep}}(\lambda, h)\,\mathrm{d}h, \tag{5}$$

where h_0 is the surface altitude, h_1 is usually the top of the atmosphere (e.g. when measured by a Sun photometer) and λ the wavelength. Here, h_1 is the height of the highest profile point reached by the aircraft.

To obtain the AOD from the in-situ measurements the dry ground-based measured $\sigma_{\mathrm{sp,dry}}$ (nephelometer) and $\sigma_{\mathrm{ap,dry}}$ (aethalometer) were first transformed to the respective AERONET wavelength using the Ångström law:

$$\sigma_{\mathrm{sp}}(\lambda) = k\lambda^{-\alpha_{\mathrm{sp}}}, \tag{6}$$

where k is the turbidity coefficient and α the Ångström exponent. Equation (6) can be formulated for $\sigma_{\mathrm{ap,dry}}$ in an analogous way. The sum of $\sigma_{\mathrm{sp,dry}}$ and $\sigma_{\mathrm{ap,dry}}$ yields the particle light extinction coefficient $\sigma_{\mathrm{ep,dry}}$. To calculate $\sigma_{\mathrm{ep,dry}}(\lambda, h)$ at different altitudes the total particle number concentration N_{tot} as measured by the airborne CPC was used as a scaling factor $c(h)$. The in-situ AOD for the dry case then calculates as follows

$$\mathrm{AOD}^{\text{in-situ}}_{\mathrm{dry}}(\lambda) = \int_{h_0}^{h_1} c(h)\,\sigma^{\text{ground}}_{\mathrm{ep,\,dry}}(\lambda)\,\mathrm{d}h \quad \text{with} \quad c(h) = \frac{N_{\mathrm{tot}}(h)}{N_{\mathrm{tot}}(h_0)}. \tag{7}$$

For the ambient in-situ AOD, the particle hygroscopic growth at RH of the different altitudes was now taken into account by using the ground-based measured $f(\mathrm{RH})$ and assuming that it does only depend on RH. This assumption means that the particle

ACPD
15, 3327–3379, 2015

chemical composition and intensive size distribution parameter do not change with altitude. Eq. (7) then changes to

$$\mathrm{AOD}_{\mathrm{amb.}}^{\mathrm{in\text{-}situ}}(\lambda) = \int_{h_0}^{h_1} c(h)\left(f(\mathrm{RH},\lambda)\sigma_{\mathrm{sp,\,dry}}^{\mathrm{ground}}(\lambda) + \sigma_{\mathrm{ap,\,dry}}^{\mathrm{ground}}(\lambda)\right)\mathrm{d}h. \quad (8)$$

Note that the absorption coefficient is assumed not to change with RH. This is a reasonable assumption at Hyytiälä due to the dominance of the light scattering (i.e. campaign average for the single scattering albedo $\omega_0 = 0.94 \pm 0.03$ at $\lambda = 525$ nm) and thus small caused error. The f(RH) is linearly inter- or extrapolated to the AERONET wavelengths.

Two example profiles showing the in-situ derived profiles are presented in Fig. 8. For comparison, the ambient extinction coefficient measured at the ground is shown together with the RH-profile. As a test for the variability, the calculations were repeated by using the 25th and 75th percentiles as lower and upper boundary, respectively. In the first example, the top of the ML is clearly seen at around 1500 m. The particle light extinction coefficient sharply decreases above the ML. The RH-effect is significant but not very strong due to the low hygroscopicity of the organic-dominated aerosol at Hyytiälä and the low RH profile during that time of day (RH varied within the ML between 50 and 70 % while it decreased to 20 % above 2000 m). Integrating the ambient extinction coefficient profile yields an $\mathrm{AOD}_{\mathrm{amb.}}^{\mathrm{in\text{-}situ}}$ of 0.018 at $\lambda = 500$ nm, while the AERONET Sun photometer measured a value of 0.055. The second profile example (Fig. 8b) shows the result for the 2 June, where no clear ML transition can be observed. The extinction coefficient still is elevated even at the maximum flight level of 2700 m. An integration of the ambient extinction coefficient profile gives an $\mathrm{AOD}_{\mathrm{amb.}}^{\mathrm{in\text{-}situ}}$ of 0.1 at $\lambda = 500$ nm, while the Sun photometer measured a value of 0.37. The time series for all profile retrieved AOD-values and the AERONET measured ones are depicted in Fig. 9 together with the maximum flight altitude. The in-situ derived values follow the course in time of the direct AOD values of the Sun photometer. However, they are 2–3 times

ACPD
15, 3327–3379, 2015

smaller than the directly obtained ones. The AOD increases in the beginning of June due to long-rang transport of mineral dust in elevated layers (see Sect. 6.3). The WetNeph was not in continuous operation between 8 and 15 June 2013 due to computer failures and thus the ambient $AOD_{amb.}^{in\text{-}situ}$ was not retrieved for this period.

The calculations were done for all Sun photometer wavelengths. A summary of this comparison is given in Fig. 10, where the R^2 and the intercept and slope of a linear least squares regression are shown for each wavelength. The in-situ derived and directly measured AODs are clearly correlated. The correlation decreases with increasing wavelength. The linear regression for each wavelength shows no large offset, but a slope of 0.5 for λ = 340 nm which similar to R^2 decreases with increasing wavelength (e.g. a slope of 0.03 for 1064 nm). One should keep in mind that a slope of 0.5 is equivalent to an underestimation of the AOD by the in-situ measurements of a factor of 2, while for the upper end of the spectrum this is even an underestimation of a factor of around 30. The following hypotheses are brought forward to explain the clear and unexpected disagreement between in-situ derived and directly measured AOD:

1. Inconsistencies within the in-situ measurements
2. Missing coarse mode particles ($D_p > 1\,\mu m$) and general sampling losses within the ground-based in-situ measurements
3. Removal by dry deposition within the canopy
4. Aerosol layers above the maximum flight altitude

The hypothesis will be discussed in detail in the following section.

ACPD
15, 3327–3379, 2015

6 Discussion

6.1 Consistency of in-situ measurements: optical closure study

To proof the consistency of the optical and microphysical aerosol in-situ measurements, a closure study based on Mie theory (Bohren and Huffman, 2004) was performed. The particles were assumed to be spherical, homogeneous, and internally mixed. As input, the particle number size distribution measured by the DMPS and APS was used. The complex refractive index (RI) was inverted from the dry scattering (nephelometer) and absorption coefficient (aethalometer) measurements and the measured particle number size distribution using Mie theory (Zieger et al., 2010). Only the measurements from the continuous aerosol monitoring program were used for the retrieval since they were also located inside the aerosol cottage. The calculation was done incorporating the TSI nephelometer illumination sensitivity and the specific scattering angles to avoid the truncation error (Anderson et al., 1996). For $\lambda = 450$ nm a mean value for the RI of $(1.56 \pm 0.07) + (0.008 \pm 0.005)i$ was calculated, while $(1.53 \pm 0.06) + (0.008 \pm 0.005)i$ and $(1.50 \pm 0.07) + (0.008 \pm 0.005)i$ were calculated for $\lambda = 550$ nm and $\lambda = 700$ nm, respectively. These retrieved real parts of the RI for Hyytiälä are close to the values of ammonium sulphate (e.g. $1.536 + 10^{-7}i$ at $\lambda = 450$ nm; Toon et al., 1976). The result of the Mie calculations is shown in Fig. 11a, where the relative differences between prediction (Mie calculation) and measurement is shown for all nephelometer wavelengths. The monitoring nephelometer (located in the cottage) is in almost perfect agreement to the calculation which is reasonable since the same measurement was used to retrieve the RI. However, the little variation proves that it is justified to use an average and fixed RI for each wavelength for the entire period. The calculated $\sigma_{sp,dry}$ for the dry nephelometer used within the WetNeph system (located in the campaign containers) are clearly underestimated by the model calculations (on average 8–30 %, see Fig. 11a). This corresponds to general differences between the dry monitoring nephelometer in the cottage measuring less particle light scattering than the reference nephelometer of the WetNeph located inside the container (see Fig. 11b). The lower measured scattering

ACPD
15, 3327–3379, 2015

coefficients of the cottage nephelometer are in correspondence to the underestimation of the measured particle number size distribution, which is an input to the Mie calculation. Therefore, particle number concentration and light scattering measurements of the monitoring measurement inside the cottage were effected by the same loss effect. Almost the same result is obtained when the RI of ammonium sulphate is taken. Small parts of the disagreement could come from general calibration issues of the nephelometers used in the WetNeph set-up. The larger variation of the WetNeph reference nephelometer (the error bars denote the 25th and 75th percentile values) suggest that the container site experienced more variation in aerosol concentration compared to the cottage site inside the forest.

The differences in the scattering coefficients, as extensive properties, cancel out when the scattering enhancement as an intensive property is calculated. In a first test, the hygroscopic growths factors g(RH) (Eq. 3) of the HTDMA were taken (details on the f(RH)-calculation can be found in Zieger et al., 2013). The g(RH)-values were interpolated between the measured dry diameters of D_p = 30 and 145 nm. Above 145 nm, the values of g(RH) were assumed to be the same as the one measured at D_p = 145 nm (similar for D_p = 30 nm). The calculated values of f(RH) using the HTDMA measurements lie on average within the range of the measured values (Fig. 11a). A slight disagreement for the larger wavelengths (on average 12 % at 635 nm) is found. As second test, the values of g(RH) were calculated using the ACSM and EC/OC measurements. The value for pure organics was first assumed to be g_{org}(RH = 90 %) = 1.2 (Fierz-Schmidhauser et al., 2010a; Zieger et al., 2014) and secondly assumed to be g_{org}(RH = 90 %) = 1.05, a value recently derived for isoprene dominated organics at Hyytiälä (Riipinen et al., 2014). The calculated values using the original value of g_{org}(RH = 90 %) = 1.2 are systematically higher than the direct measurements (≈ 30 %), while the lower value of g_{org}(RH = 90 %) = 1.05 delivers an improved agreement. This points towards the importance of the hygroscopic growth factor, which is especially for low hygroscopic substances important when calculating f(RH) (see Fig. A1 in Zieger et al., 2013).

ACPD
15, 3327–3379, 2015

Summarizing the optical closure study, one can conclude that the different in-situ measurements provide consistent results. However, the differences found in the scattering coefficients measured by the monitoring and reference nephelometers point towards losses. Smaller differences can additionally be explained by the simplified assumptions taken for the Mie calculations (e.g. internal mixture, homogeneous and spherical particles, no size dependence of the refractive index, specific values for g(RH)).

6.2 Particle losses

The Sun photometer was placed on a tower above the forest canopy, while the in-situ measurements were performed on ground below the canopy. Particles may have been lost within the canopy by dry deposition before reaching the inlet (Grönholm et al., 2007; Buzorius et al., 2003; Petroff et al., 2008), which includes removal through Brownian diffusion (mainly for fine mode particles below $D_p < 100$ nm) or through impaction or interception (mainly for coarse mode particles above $D_p > 1000$ nm). Grönholm et al. (2009) performed aerosol flux measurements using the eddy covariance technique at Hyytiälä and found that only 35 % of the particles penetrated through the canopy at low wind speeds. At higher wind speeds and correspondingly stronger turbulent conditions only 10 % of all particles reached the ground. The study by Grönholm et al. (2009) was performed in spring, while our measurements were done in summer months with probably more turbulence and thus higher deposition losses. In addition, particle losses could have also occurred within the inlet and tubing itself. However, this is rather unlikely, since the optical closure study has shown the consistency of the optical and microphysical aerosol measurements.

Figure 12a shows the average particle number size distribution measured at the ground and by the aircraft within the lowest layer. For small particles below 100 nm, the aircraft measured on average higher concentrations (up to 40 %) than the ground-based instrument. This was also seen in the CPC comparison (Fig. 7b). However, for the optically important size range above 100 nm, both size distributions agree sur-

ACPD
15, 3327–3379, 2015

prisingly well. Figure 12b depicts the scattering size distribution calculated using the measured size distributions and Mie theory. Here, both size distribution measurements agree until the maximum diameter of the aircraft SMPS is reached. Unfortunately, above $D_p > 260$ nm, the aircraft did not record the size distribution and thus missed information on the optically important part of the aerosol size spectrum.

The spectral course of the linear regressions and the optically decrease of the R^2 with increasing wavelength (see Fig. 10) point towards an influence of large particles which are not sufficiently sampled by the in-situ instruments. Figure 13 shows the calculated scattering coarse mode fraction (defined as the scattering coefficient for particles above $D_p > 1$ µm divided by the total scattering coefficient both calculated using Mie theory) for all wavelengths used in the Sun photometer measurements. The calculation was done for all time periods with corresponding profiles using the particle number size distribution measurement on the ground. With increasing wavelength more light scattering will be due to coarse mode particles. At $\lambda = 1020$ nm, for example, it is already 50 % for the here measured aerosol. A few losses of supermicron particles can therefore explain the observed differences. Again, a sensitivity analysis using Mie theory and the measured ground-based size distribution showed that increasing the number concentration of the coarse mode by a factor of 5 increased the slope of the linear regression (see Fig. 10c) for all wavelengths to 0.5. The slope for the smaller wavelengths did not change and remained at around 0.5, which points towards an additional loss effect of fine mode particles (260 nm $< D_p <$ 1 µm).

The calculations were repeated by artificially increasing the fine and coarse mode number concentrations separately. The spectral course of the slope (see Fig. 10c) would loose its decreasing spectral behaviour and reach a flat line if the coarse mode number concentration ($D_p > 1$ µm) would be multiplied by a factor of 5 (still showing a mean value of 0.5). The magnitude would increase to around 1, if the fine mode number concentration ($D_p < 1$ µm) would be increased by a factor of 3. However, the comparison of airborne and ground-based CPC showed only a small increased number concentration of the airborne CPC (slope 1.16, see Fig. 7).

ACPD
15, 3327–3379, 2015

The AOD for the fine mode fraction ($D_p < 1\,\mu m$) was estimated by taking the measured particle number size distribution at ground and applying Mie theory (taking the RI from the Mie inversion, see Sect. 6.1) which results in the extinction coefficient for submicrometer particles only. The calculation of in-situ AOD for the fine mode fraction followed in the same manner as described above (using Eq. 8). The comparison of the derived values to the AERONET inverted fine mode AOD is shown in Fig. 14. A high correlation was found ($R^2 = 0.84$) and a linear least-squares regression revealed that the AERONET values were significantly higher (slope of 1.53) compared to the in-situ derived values. Again, this indicates that besides the missing coarse mode also the loss of fine mode particles contributed to the found disagreement. These particles could have been fine mode particles above the maximum flight altitude (see Sect. 6.3) or particles possibly lost through dry deposition within the canopy.

6.3 Elevated layers

As discussed above, the airborne sampling was only performed to a maximum altitude of 3.2 km. Thus, elevated layers contributing to the columnar AOD could have been missed by the aircraft. The time series of the AOD in Fig. 9b already showed an unusual increase of the AOD (to 0.35 at $\lambda = 500$ nm; starting approximately on the 2 June 2013) compared to the average values measured at Hyytiälä (0.12 ± 0.04, Aaltonen et al., 2012). Figure 15 shows lidar profiles of the aerosol backscatter coefficient (at $\lambda = 1064$ nm) recorded at Kuopio during the airborne campaign. While there are no significant elevated layers before the 28 May, clear elevated layers are seen above 3000 m from the 30 May until the 3 June. Air mass back trajectories showed that the air originated from the Arabian peninsula and thus could consist of layers of mineral dust particles. In addition, the depolarization channel showed values indicative for non-spherical particles. Figure 15 also gives the percental contribution from the layer above 3 km and below 7 km to the total AOD derived by the lidar. For the period before the 2 June 15–25 % of the AOD was attributed to aerosol particles in elevated layers, while

ACPD
15, 3327–3379, 2015

elevated layers contributed between 60 and 80 % to the AOD between 2 and 3 June (assuming a constant lidar ratio).

7 Conclusions

The effect of water uptake on the particle light scattering coefficient was investigated at a boreal site using a humidified nephelometer system. Compared to other major aerosol types the aerosol light scattering enhancement factor $f(\mathrm{RH})$ shows low values with little variation (at RH = 85 % and $\lambda = 525$ nm a mean value of 1.63 ± 0.22). This is attributed to the dominance of the organic mass within the submicron range, to which $f(\mathrm{RH})$ clearly correlates ($R^2 = 0.77$–0.79). $f(\mathrm{RH})$ can thus be estimated using the continuous chemical composition measurements if no direct $f(\mathrm{RH})$ measurement is available for the aerosol found during summer months at Hyytiälä. A trajectory analysis revealed that higher values of $f(\mathrm{RH})$ and higher inorganic mass fractions at Hyytiälä were due to hygroscopic sea spray particles transported to the site.

The measurement of the $f(\mathrm{RH})$ allowed to estimate the particle light extinction coefficient at ambient RH. This was then used to extrapolate the ground-based in-situ parameters to the atmospheric column using aircraft measurements of the particle number concentration as a scaling factor. The in-situ derived AOD showed a high correlation for the UV and visible wavelengths when compared to direct measurements of a Sun photometer ($R^2 \approx 0.9$ for $\lambda = 400$ nm to $R^2 \approx 0.6$ for $\lambda = 1000$ nm), however, a clear underestimation of the AOD by at least a factor of 2 was found. To investigate the reasons for this disagreement, different hypothesis were brought forward and discussed. An optical closure study showed the validity of the ground-based in-situ measurements and showed that a lower hygroscopic growth of the organic compounds resulted in an improved agreement with respect to $f(\mathrm{RH})$. The discrepancy of the in-situ derived AOD increased for larger wavelengths pointing towards an underestimation of coarse mode particles which might have been removed by the canopy or were not sufficiently sampled by the in-situ instruments. In addition, elevated layers observed by

ACPD
15, 3327–3379, 2015

a lidar at Kuopio can explain part of the found disagreement. The remaining differences are speculated to come from dry deposition within the canopy.

This work demonstrated the difficulties faced when using ground based in-situ measurements for the validation of remote sensing (e.g. Sun photometer and later even satellite) measurements. Consequently, more research work and improved measurements are needed for integrating in-situ measurements for the validation or comparison of remote sensing retrievals. For sampling sites located in forest environments, the removal by the canopy of fine and coarse mode particles has to be included when analysing time series of aerosol optical properties.

Acknowledgements. The research leading to these results has received funding from the European Union Seventh Framework Programme (FP7/2007–2013) under grant agreement no. 262254. The work was supported by US Office of Science (BER), Department of Energy via project "Biogenic Aerosols – Effects on Clouds and Climate (BAECC)", European Union (BACCHUS: 603445, PEGASOS: 265148), Nordforsk via the Nordic Center of Excellence CRAICC, and the Academy of Finland via the "Center of Excellence in Atmospheric Sciences" (project no. 272041). We thank Janne Levula and the technical personal at Hyytiälä for their support. Paul Zieger was supported by a PostDoc fellowship from the Swiss National Science Foundation (grant no. P300P2_147776).

References

Aaltonen, V., Rodriguez, E., Kazadzis, S., Arola, A., Amiridis, V., Lihavainen, H., and de Leeuw, G.: On the variation of aerosol properties over Finland based on the optical columnar measurements, Atmos. Res., 116, 46–55, doi:10.1016/j.atmosres.2011.07.014, 2012. 3339, 3352

Allan, J., Jimenez, J., Williams, P., Alfarra, M., Bower, K., Jayne, J., Coe, H., and Worsnop, D.: Quantitative sampling using an Aerodyne aerosol mass spectrometer 1. Techniques of data interpretation and error analysis, J. Geophys. Res., 108, 4090, doi:10.1029/2002JD002358, 2003. 3336

Allan, J., Delia, A., Coe, H., Bower, K., Alfarra, M., Jimenez, J., Middlebrook, A., Drewnick, F., Onasch, T., Canagaratna, M., Jayne, J., and Worsnop, D.: A generalised method for the

ACPD
15, 3327–3379, 2015

extraction of chemically resolved mass spectra from Aerodyne aerosol mass spectrometer data, J. Aerosol Sci., 35, 909–922, 2004. 3336

Allan, J. D., Alfarra, M. R., Bower, K. N., Coe, H., Jayne, J. T., Worsnop, D. R., Aalto, P. P., Kulmala, M., Hyötyläinen, T., Cavalli, F., and Laaksonen, A.: Size and composition measurements of background aerosol and new particle growth in a Finnish forest during QUEST 2 using an Aerodyne Aerosol Mass Spectrometer, Atmos. Chem. Phys., 6, 315–327, doi:10.5194/acp-6-315-2006, 2006. 3331

Althausen, D., Engelmann, R., Baars, H., Heese, B., Ansmann, A., Müller, D., and Komppula, M.: Portable Raman lidar PollyXT for automated profiling of aerosol backscatter, extinction, and depolarization, J. Atmos. Ocean. Tech., 26, 2366–2378, 2009. 3339

Anderson, T., Covert, D., Marshall, S., Laucks, M., Charlson, R., Waggoner, A., Ogren, J., Caldow, R., Holm, R., Quant, F., Sem, G., Wiedensohler, A., Ahlquist, N., and Bates, T.: Performance characteristics of a high-sensitivity, three-wavelength, total scatter/backscatter nephelometer, J. Atmos. Ocean. Tech., 13, 967–986, 1996. 3348

Bohren, C. and Huffman, D.: Absorption and Scattering of Light by Small Particles, WILEY-VCH Verlag GmbH & Co. KGaA, Weinheim, Germany, 2004. 3348

Buzorius, G., Rannik, Ü., Nilsson, E., Vesala, T., and Kulmala, M.: Analysis of measurement techniques to determine dry deposition velocities of aerosol particles with diameters less than 100 nm, J. Aerosol Sci., 34, 747–764, 2003. 3350

Canagaratna, M., Jayne, J., Jimenez, J., Allan, J., Alfarra, M., Zhang, Q., Onasch, T., Drewnick, F., Coe, H., Middlebrook, A., Delia, A., Williams, L., Trimborn, A., Northway, M., DeCarlo, P., Kolb, C., Davidovits, P., and Worsnop, D.: Chemical and microphysical characterization of ambient aerosols with the Aerodyne aerosol mass spectrometer, Mass Spectrom. Rev., 26, 185–222, 2007. 3336

Carrico, C., Rood, M., and Ogren, J.: Aerosol light scattering properties at Cape Grim, Tasmania, during the first Aerosol Characterization Experiment (ACE 1), J. Geophys. Res., 103, 16565–16574, doi:10.1029/98JD00685, 1998. 3331

Carrico, C., Rood, M., Ogren, J., Neusüß, C., Wiedensohler, A., and Heintzenberg, J.: Aerosol optical properties at Sagres, Portugal, during ACE-2, Tellus B, 52, 694–715, doi:10.1034/j.1600-0889.2000.00049.x, 2000. 3331

Carrico, C., Kus, P., Rood, M., Quinn, P., and Bates, T.: Mixtures of pollution, dust, sea salt, and volcanic aerosol during ACE-Asia: radiative properties as a function of relative humidity, J. Geophys. Res., 108, 8650, doi:10.1029/2003JD003405, 2003. 3331, 3334

ACPD
15, 3327–3379, 2015

Clarke, A. D. and Howell, S. and Quinn, P. K. and Bates, T. S. and Ogren, J. A. and Andrews, E. and Jefferson, A. and Massling, A. and Mayol-Bracero, O. and Maring, H. and Savoie, D., and Cass, G.: INDOEX aerosol: A comparison and summary of chemical, microphysical, and optical properties observed from land, ship, and aircraft, J. Geophys. Res., 107, 8033, doi:10.1029/2001JD000572, 2002. 3334

Collins, D. R., Flagan, R. C., and Seinfeld, J. H.: Improved Inversion of Scanning DMA Data, Aerosol Sci. Tech., 36, 1–9, doi:10.1080/027868202753339032, 2002. 3338

Covert, D. S., Charlson, R., and Ahlquist, N.: A study of the relationship of chemical composition and humidity to light scattering by aerosols, J. Appl. Meteorol., 11, 968–976, 1972. 3331

Draxler, R.: Description of the HYSPLIT4 Modeling System, NOAA Technical Memorandum ERL ARL-224 edn., Air Resources Laboratory, Silver Spring, Maryland, 2004. 3340

Draxler, R. R. and Hess, G.: An overview of the HYSPLIT_4 modelling system for trajectories, Aust. Meteorol. Mag., 47, 295–308, 1998. 3340

Dubovik, O., Sinyuk, A., Lapyonok, T., Holben, B. N., Mishchenko, M., Yang, P., Eck, T. F., Volten, H., Muñoz, O., Veihelmann, B., van der Zande, W. J., Leon, J.-F., Sorokin, M., and Slutsker, I.: Application of spheroid models to account for aerosol particle nonsphericity in remote sensing of desert dust, J. Geophys. Res., 111, 1–34, doi:10.1029/2005JD006619, 2006. 3339

Ehn, M., Petäjä, T., Aufmhoff, H., Aalto, P., Hämeri, K., Arnold, F., Laaksonen, A., and Kulmala, M.: Hygroscopic properties of ultrafine aerosol particles in the boreal forest: diurnal variation, solubility and the influence of sulfuric acid, Atmos. Chem. Phys., 7, 211–222, doi:10.5194/acp-7-211-2007, 2007. 3331

Engelmann, R., Althausen, D., Heese, B., Baars, H., and Komppula, M.: Recent upgrades of the multiwavelength polarization Raman lidar PollyXT, in: Reviewed and Revised Papers of the 26th International Laser Radar Conference, Porto Heli, Greece, 25–29 June 2012, 171–175, 2012. 3339

Esteve, A. R., Ogren, J. A., Sheridan, P. J., Andrews, E., Holben, B. N., and Utrillas, M. P.: Sources of discrepancy between aerosol optical depth obtained from AERONET and in-situ aircraft profiles, Atmos. Chem. Phys., 12, 2987–3003, doi:10.5194/acp-12-2987-2012, 2012. 3331

Ferrare, R., Melfi, S., Whiteman, D., Evans, K., and Leifer, R.: Raman lidar measurements of aerosol extinction and backscattering 1. Methods and comparisons, J. Geophys. Res., 103, 19663–19672, doi:10.1029/98JD01646, 1998. 3331

ACPD
15, 3327–3379, 2015

Fierz-Schmidhauser, R., Zieger, P., Gysel, M., Kammermann, L., DeCarlo, P. F., Baltensperger, U., and Weingartner, E.: Measured and predicted aerosol light scattering enhancement factors at the high alpine site Jungfraujoch, Atmos. Chem. Phys., 10, 2319–2333, doi:10.5194/acp-10-2319-2010, 2010a. 3331, 3349

Fierz-Schmidhauser, R., Zieger, P., Vaishya, A., Monahan, C., Bialek, J., O'Dowd, C. D., Jennings, S. G., Baltensperger, U., and Weingartner, E.: Light scattering enhancement factors in the marine boundary layer (Mace Head, Ireland), J. Geophys. Res., 115, D20204, doi:10.1029/2009jd013755, 2010b. 3331

Fierz-Schmidhauser, R., Zieger, P., Wehrle, G., Jefferson, A., Ogren, J. A., Baltensperger, U., and Weingartner, E.: Measurement of relative humidity dependent light scattering of aerosols, Atmos. Meas. Tech., 3, 39–50, doi:10.5194/amt-3-39-2010, 2010c. 3331, 3333, 3334

Fitzgerald, J., Hoppel, W., and Vietti, M.: The size and scattering coefficient of urban aerosol particles at Washington, DC as a function of relative humidity, J. Atmos. Sci., 39, 1838–1852, 1982. 3331

Gasso, S., Hegg, D., Covert, D., Collins, D., Noone, K., Öström, E., Schmid, B., Russell, P., Livingston, J., Durkee, P., and Jonsson, H.: Influence of humidity on the aerosol scattering coefficient and its effect on the upwelling radiance during ACE-2, Tellus B, 52, 546–567, 2000. 3331

Grönholm, T., Aalto, P. P., Hiltunen, V., Rannik, Ü., Rinne, J., Laakso, L., Hyvönen, S., Vesala, T., and Kulmala, M.: Measurements of aerosol particle dry deposition velocity using the relaxed eddy accumulation technique, Tellus B, 59, 381–386, 2007. 3350

Grönholm, T., Launiainen, S., Ahlm, L., Mårtensson, E., Kulmala, M., Vesala, T., and Nilsson, E.: Aerosol particle dry deposition to canopy and forest floor measured by two-layer eddy covariance system, J. Geophys. Res., 114, D04202, doi:10.1029/2008JD010663, 2009. 3350

Hämeri, K., Väkevä, M., Aalto, P., Kulmala, M., Swietlicki, E., Zhou, J., Seidl, W., Becker, E., and O'Dowd, C.: Hygroscopic and CCN properties of aerosol particles in boreal forests, Tellus B, 53, 359–379, 2001. 3331

Hari, P. and Kulmala, M.: Station for Measuring Ecosystem-Atmosphere Relations (SMEAR II), Boreal Environ. Res., 10, 315–322, 2005. 3332

Hirsikko, A., O'Connor, E. J., Komppula, M., Korhonen, K., Pfüller, A., Giannakaki, E., Wood, C. R., Bauer-Pfundstein, M., Poikonen, A., Karppinen, T., Lonka, H., Kurri, M., Heinonen, J., Moisseev, D., Asmi, E., Aaltonen, V., Nordbo, A., Rodriguez, E., Lihavainen, H.,

ACPD
15, 3327–3379, 2015

Laaksonen, A., Lehtinen, K. E. J., Laurila, T., Petäjä, T., Kulmala, M., and Viisanen, Y.: Observing wind, aerosol particles, cloud and precipitation: Finland's new ground-based remote-sensing network, Atmos. Meas. Tech., 7, 1351–1375, doi:10.5194/amt-7-1351-2014, 2014. 3339

Holben, B., Eck, T., Slutsker, I., Tanre, D., Buis, J., Setzer, A., Vermote, E., Reagan, J., Kaufman, Y., Nakajia, T., Lavenu, F., Jankowiak, I., and Smirnov, A.: AERONET – A federated instrument network and data archive for aerosol characterization, Remote Sens. Environ., 66, 1–6, 1998. 3339

Hong, J., Häkkinen, S. A. K., Paramonov, M., Äijälä, M., Hakala, J., Nieminen, T., Mikkilä, J., Prisle, N. L., Kulmala, M., Riipinen, I., Bilde, M., Kerminen, V.-M., and Petäjä, T.: Hygroscopicity, CCN and volatility properties of submicron atmospheric aerosol in a boreal forest environment during the summer of 2010, Atmos. Chem. Phys., 14, 4733–4748, doi:10.5194/acp-14-4733-2014, 2014. 3334

Karanasiou, A., Diapouli, E., Cavalli, F., Eleftheriadis, K., Viana, M., Alastuey, A., Querol, X., and Reche, C.: On the quantification of atmospheric carbonate carbon by thermal/optical analysis protocols, Atmos. Meas. Tech., 4, 2409–2419, doi:10.5194/amt-4-2409-2011, 2011. 3337

Koloutsou-Vakakis, S., Carrico, C., Kus, P., Rood, M., Li, Z., Shrestha, R., Ogren, J., Chow, J., and Watson, J.: Aerosol properties at a midlatitude Northern Hemisphere continental site, J. Geophys. Res., 106, 3019–3032, 2001. 3331

Kotchenruther, R. and Hobbs, P.: Humidification factors of aerosols from biomass burning in Brazil, J. Geophys. Res., 103, 32081–32089, doi:10.1029/98JD00340, 1998. 3331

Leino, K., Riuttanen, L., Nieminen, T., Dal Maso, M., Väänänen, R., Pohja, T., Keronen, P., Järvi, L., Aalto, P. P., Virkkula, A., Kerminen, V.-M., Petäjä, T., and Kulmala, M.: Biomass-burning smoke episodes in Finland from eastern European wildfires, Boreal Environ. Res., 19, 275–292, 2014. 3338

McInnes, L., Bergin, M., Ogren, J., and Schwartz, S.: Apportionment of light scattering and hygroscopic growth to aerosol composition, Geophys. Res. Lett., 25, 513–516, doi:10.1029/98GL00127, 1998. 3331

McNaughton, C., Clarke, A., Howell, S., Pinkerton, M., Anderson, B., Thornhill, L., Hudgins, C., Winstead, E., Dibb, J., Scheuer, E., and Maring, H.: Results from the DC-8 Inlet Characterization Experiment (DICE): airborne versus surface sampling of mineral dust and sea salt aerosols, Aerosol Sci. Tech., 41, 136–159, doi:10.1080/02786820601118406, 2007. 3338

ACPD
15, 3327–3379, 2015

Morgan, W. T., Allan, J. D., Bower, K. N., Esselborn, M., Harris, B., Henzing, J. S., Highwood, E. J., Kiendler-Scharr, A., McMeeking, G. R., Mensah, A. A., Northway, M. J., Osborne, S., Williams, P. I., Krejci, R., and Coe, H.: Enhancement of the aerosol direct radiative effect by semi-volatile aerosol components: airborne measurements in North-Western Europe, Atmos. Chem. Phys., 10, 8151–8171, doi:10.5194/acp-10-8151-2010, 2010. 3331

Müller, T., Laborde, M., Kassell, G., and Wiedensohler, A.: Design and performance of a three-wavelength LED-based total scatter and backscatter integrating nephelometer, Atmos. Meas. Tech., 4, 1291–1303, doi:10.5194/amt-4-1291-2011, 2011. 3333

Ng, N., Herndon, S., Trimborn, A., Canagaratna, M., Croteau, P., Onasch, T., Sueper, D., Worsnop, D., Zhang, Q., Sun, Y., and Jayne, J.: An Aerosol Chemical Speciation Monitor (ACSM) for routine monitoring of the composition and mass concentrations of ambient aerosol, Aerosol Sci. Tech., 45, 780–794, 2011. 3336

Pan, X. L., Yan, P., Tang, J., Ma, J. Z., Wang, Z. F., Gbaguidi, A., and Sun, Y. L.: Observational study of influence of aerosol hygroscopic growth on scattering coefficient over rural area near Beijing mega-city, Atmos. Chem. Phys., 9, 7519–7530, doi:10.5194/acp-9-7519-2009, 2009. 3331

Petäjä, T., Kerminen, V.-M., Hämeri, K., Vaattovaara, P., Joutsensaari, J., Junkermann, W., Laaksonen, A., and Kulmala, M.: Effects of SO_2 oxidation on ambient aerosol growth in water and ethanol vapours, Atmos. Chem. Phys., 5, 767–779, doi:10.5194/acp-5-767-2005, 2005. 3331

Peterson, M. R. and Richards, M. H.: Thermal-optical-transmittance analysis for organic, elemental, carbonate, total carbon, and OCX2 in PM2. 5 by the EPA/NIOSH method, in: Proceedings, Symposium on Air Quality Measurement Methods and Technology-2002, 83–1, Air and Waste Management Association, Pittsburgh, PA, San Francisco, CA Date: November 2002 Session 5, Paper #83, 2002. 3337

Petroff, A., Mailliat, A., Amielh, M., and Anselmet, F.: Aerosol dry deposition on vegetative canopies. Part I: Review of present knowledge, Atmos. Environ., 42, 3625–3653, 2008. 3350

Petzold, A., Ogren, J. A., Fiebig, M., Laj, P., Li, S.-M., Baltensperger, U., Holzer-Popp, T., Kinne, S., Pappalardo, G., Sugimoto, N., Wehrli, C., Wiedensohler, A., and Zhang, X.-Y.: Recommendations for reporting "black carbon" measurements, Atmos. Chem. Phys., 13, 8365–8379, doi:10.5194/acp-13-8365-2013, 2013. 3335

Pilat, M. and Charlson, R.: Theoretical and optical studies of humidity effects on the size distribution of a hygroscopic aerosol, J. Rech. Atmos., 2, 166–170, 1966. 3331

ACPD
15, 3327–3379, 2015

Pilinis, C., Pandis, S., and Seinfeld, J.: Sensitivity of direct climate forcing by atmospheric aerosols to aerosol size and composition, J. Geophys. Res., 100, 18739–18754, doi:10.1029/95JD02119, 1995. 3330

Riipinen, I., Rastak, N., and Pandis, S. N.: Connecting the solubility and CCN activation of complex organic aerosols: a theoretical study using the Solubility Basis Set (SBS), Atmos. Chem. Phys. Discuss., 14, 28523–28569, doi:10.5194/acpd-14-28523-2014, 2014. 3349

Schobesberger, S., Väänänen, R., Leino, K., Virkkula, A., Backman, J., Pohja, T., Siivola, E., Franchin, A., Mikkilä, J., Paramonov, M., Aalto, P., Krejci, R., Petäjä, T., and Kulmala, M.: Airborne measurements over the boreal forest of southern Finland during new particle formation events in 2009 and 2010, Boreal Environ. Res., 18, 145–163, 2013. 3338

Sheridan, P., Delene, D., and Ogren, J.: Four years of continuous surface aerosol measurements from the Department of Energy's Atmospheric Radiation measurement program southern great plains cloud and radiation testbed site, J. Geophys. Res., 106, 20735–20747, 2001. 3331

Swietlicki, E., Hansson, H., Hämeri, K., Svenningsson, B., Massling, A., McFiggans, G., McMurry, P., Petäjä, T., Tunved, P., Gysel, M., Topping, D., Weingartner, E., Baltensperger, U., Rissler, J., Wiedensohler, A., and Kulmala, M.: Hygroscopic properties of submicrometer atmospheric aerosol particles measured with H-TDMA instruments in various environments – a review, Tellus B, 60, 432–469, 2008. 3331

Tesche, M., Zieger, P., Rastak, N., Charlson, R. J., Glantz, P., Tunved, P., and Hansson, H.-C.: Reconciling aerosol light extinction measurements from spaceborne lidar observations and in situ measurements in the Arctic, Atmos. Chem. Phys., 14, 7869–7882, doi:10.5194/acp-14-7869-2014, 2014. 3331

Titos, G., Jefferson, A., Sheridan, P. J., Andrews, E., Lyamani, H., Alados-Arboledas, L., and Ogren, J. A.: Aerosol light-scattering enhancement due to water uptake during the TCAP campaign, Atmos. Chem. Phys., 14, 7031–7043, doi:10.5194/acp-14-7031-2014, 2014a. 3331

Titos, G., Lyamani, H., Cazorla, A., Sorribas, M., Foyo-Moreno, I., Wiedensohler, A., and Alados-Arboledas, L.: Study of the relative humidity dependence of aerosol light-scattering in southern Spain, Tellus B, 66, 24536, doi:10.3402/tellusb.v66.24536, 2014b. 3331

Toon, O., Pollack, J., and Khare, B.: The optical constants of several atmospheric aerosol species: ammonium sulfate, aluminum oxide, and sodium chloride, J. Geophys. Res., 81, 5733–5748, doi:10.1029/JC081i033p05733, 1976. 3348

ACPD
15, 3327–3379, 2015

Väänänen, R., Krejci, R., Manninen, H., Nieminen, T., Yli-Juuti, T., Kangasluoma, J., Pohja, T., Aalto, P., Petäjä, T., and Kulmala, M.: Aircraft-borne measurements over southern Finland during Pegasos spring 2013 campaign, n.a., in preparation, 2015. 3339

Vesala, T., Haataja, J., Aalto, P., Altimir, N., Buzorius, G., Garam, E., Hämeri, K., Ilvesniemi, H., Jokinen, V., Keronen, P., Lahti, T., Markkanen, T., Mäkelä, J., E., N., Palmmroth, S., Palva, L., Pohja, T., Pumpanen, J., Rannik, U., Siivola, E., Ylitalo, H., Hari, P., and Kulmala, M.: Long-term field measurements of atmosphere-surface interaction in boreal forest combining forest ecology, micrometeorology, aerosol physics and atmospheric chemistry, Trends in Heat, Mass and Mommentum Transfer, 4, 17–35, 1998. 3332

Virkkula, A., Backman, J., Aalto, P. P., Hulkkonen, M., Riuttanen, L., Nieminen, T., dal Maso, M., Sogacheva, L., de Leeuw, G., and Kulmala, M.: Seasonal cycle, size dependencies, and source analyses of aerosol optical properties at the SMEAR II measurement station in Hyytiälä, Finland, Atmos. Chem. Phys., 11, 4445–4468, doi:10.5194/acp-11-4445-2011, 2011. 3335

Voss, K., Welton, E., Quinn, P., Frouin, R., Miller, M., and Reynolds, R.: Aerosol optical depth measurements during the Aerosols99 experiment, J. Geophys. Res., 106, 20821–20831, doi:10.1029/2000JD900783, 2001. 3331

Wang, S. and Flagan, R.: Scanning electrical mobility spectrometer, Aerosol Sci. Tech., 13, 230–240, doi:10.1080/02786829008959441, 1990. 3338

Wang, W., Rood, M., Carrico, C., Covert, D., Quinn, P., and Bates, T.: Aerosol optical properties along the northeast coast of North America during the New England Air Quality Study–Intercontinental Transport and Chemical Transformation 2004 campaign and the influence of aerosol composition, J. Geophys. Res., 112, D10S23, doi:10.1029/2006JD007579, 2007. 3331

Weingartner, E., Saathoff, H., Schnaiter, M., Streit, N., Bitnar, B., and Baltensperger, U.: Absorption of light by soot particles: determination of the absorption coefficient by means of Aethalometers, J. Aerosol Sci., 34, 1445–1465, 2003. 3335

Wiedensohler, A., Birmili, W., Nowak, A., Sonntag, A., Weinhold, K., Merkel, M., Wehner, B., Tuch, T., Pfeifer, S., Fiebig, M., Fjäraa, A. M., Asmi, E., Sellegri, K., Depuy, R., Venzac, H., Villani, P., Laj, P., Aalto, P., Ogren, J. A., Swietlicki, E., Williams, P., Roldin, P., Quincey, P., Hüglin, C., Fierz-Schmidhauser, R., Gysel, M., Weingartner, E., Riccobono, F., Santos, S., Grüning, C., Faloon, K., Beddows, D., Harrison, R., Monahan, C., Jennings, S. G., O'Dowd, C. D., Marinoni, A., Horn, H.-G., Keck, L., Jiang, J., Scheckman, J., McMurry, P. H.,

ACPD
15, 3327–3379, 2015

Deng, Z., Zhao, C. S., Moerman, M., Henzing, B., de Leeuw, G., Löschau, G., and Bastian, S.: Mobility particle size spectrometers: harmonization of technical standards and data structure to facilitate high quality long-term observations of atmospheric particle number size distributions, Atmos. Meas. Tech., 5, 657–685, doi:10.5194/amt-5-657-2012, 2012. 3336

WMO/GAW: Aerosol Measurement Procedures Guidelines and Recommendations, Report No. 153, World Meteorological Organization, Geneva, Switzerland, 2003. 3330

Yan, P., Pan, X., Tang, J., Zhou, X., Zhang, R., and Zeng, L.: Hygroscopic growth of aerosol scattering coefficient: a comparative analysis between urban and suburban sites at winter in Beijing, Particuology, 7, 52–60, 2009. 3331

Zieger, P., Fierz-Schmidhauser, R., Gysel, M., Ström, J., Henne, S., Yttri, K. E., Baltensperger, U., and Weingartner, E.: Effects of relative humidity on aerosol light scattering in the Arctic, Atmos. Chem. Phys., 10, 3875–3890, doi:10.5194/acp-10-3875-2010, 2010. 3331, 3348

Zieger, P., Weingartner, E., Henzing, J., Moerman, M., de Leeuw, G., Mikkilä, J., Ehn, M., Petäjä, T., Clémer, K., van Roozendael, M., Yilmaz, S., Frieß, U., Irie, H., Wagner, T., Shaiganfar, R., Beirle, S., Apituley, A., Wilson, K., and Baltensperger, U.: Comparison of ambient aerosol extinction coefficients obtained from in-situ, MAX-DOAS and LIDAR measurements at Cabauw, Atmos. Chem. Phys., 11, 2603–2624, doi:10.5194/acp-11-2603-2011, 2011. 3331, 3334

Zieger, P., Kienast-Sjögren, E., Starace, M., von Bismarck, J., Bukowiecki, N., Baltensperger, U., Wienhold, F. G., Peter, T., Ruhtz, T., Collaud Coen, M., Vuilleumier, L., Maier, O., Emili, E., Popp, C., and Weingartner, E.: Spatial variation of aerosol optical properties around the high-alpine site Jungfraujoch (3580 m a.s.l.), Atmos. Chem. Phys., 12, 7231–7249, doi:10.5194/acp-12-7231-2012, 2012. 3331

Zieger, P., Fierz-Schmidhauser, R., Weingartner, E., and Baltensperger, U.: Effects of relative humidity on aerosol light scattering: results from different European sites, Atmos. Chem. Phys., 13, 10609–10631, doi:10.5194/acp-13-10609-2013, 2013. 3330, 3334, 3342, 3343, 3349

Zieger, P., Fierz-Schmidhauser, R., Poulain, L., Müller, T., Birmili, W., Spindler, G., Wiedensohler, A., Baltensperger, U., and Weingartner, E.: Influence of water uptake on the aerosol particle light scattering coeffcients of the Central European aerosol, Tellus B, 66, 22716, doi:10.3402/tellusb.v66.22716, 2014. 3331, 3334, 3341, 3342, 3349

ACPD
15, 3327–3379, 2015

Table 1. Mean, standard deviation (SD) and percentile values (prctl.) of the scattering enhancement factor f(RH), the magnitude γ and intercept a of the fitted humidograms.

	Mean	SD	90th prctl.	75th prctl.	Median	25th prctl.	10th prctl.
f(85 %, 450 nm)	1.53	0.24	1.90	1.64	1.47	1.35	1.26
f(85 %, 525 nm)	1.63	0.22	1.95	1.74	1.57	1.48	1.42
f(85 %, 635 nm)	1.79	0.27	2.17	1.94	1.71	1.59	1.51
γ(450 nm)	0.24	0.07	0.34	0.28	0.22	0.19	0.16
γ(525 nm)	0.25	0.07	0.35	0.29	0.24	0.20	0.17
γ(635 nm)	0.30	0.08	0.41	0.35	0.28	0.23	0.20
a(450 nm)	0.96	0.07	1.07	1.00	0.95	0.91	0.88
a(525 nm)	1.01	0.05	1.08	1.04	1.00	0.97	0.94
a(635 nm)	1.01	0.05	1.08	1.05	1.01	0.98	0.95

ACPD
15, 3327–3379, 2015

Table 2. Parameters retrieved from a linear least squares regression of the different chemical mass fractions (ACSM and EC/OC) vs. γ (fit parameter for $f(\mathrm{RH})$) for the different nephelometer wavelengths.

	Slope			Intercept			R^2		
	450 nm	525 nm	635 nm	450 nm	525 nm	635 nm	450 nm	525 nm	635 nm
Organic	−0.58	−0.58	−0.69	0.65	0.67	0.78	0.79	0.77	0.79
NH_4	1.59	1.61	1.98	0.13	0.14	0.15	0.50	0.47	0.58
SO_4	0.75	0.78	0.89	0.12	0.13	0.15	0.79	0.80	0.78
NO_3	−2.60	−2.68	−4.21	0.32	0.33	0.43	0.05	0.05	0.11
Cl	0.79	−0.99	−4.21	0.23	0.25	0.30	0.00	0.00	0.00
EC	0.38	0.29	1.72	0.22	0.24	0.26	0.01	0.00	0.03
Inorganic	0.60	0.61	0.69	0.08	0.09	0.11	0.80	0.79	0.79

ACPD
15, 3327–3379, 2015

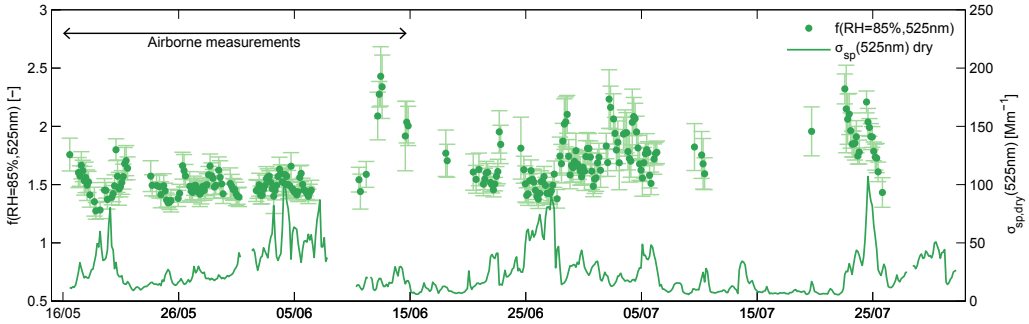

Figure 1. Time series of the scattering enhancement factor $f(\mathrm{RH})$ at RH = 85 % and λ = 525 nm (bullet points) and the dry particle light scattering coefficient at λ = 525 nm (solid line) measured at Hyytiälä. The error bars give the 95 % confidence interval. The arrow indicates the period of airborne measurements.

ACPD
15, 3327–3379, 2015

Scattering enhancement of boreal aerosol and columnar closure study

P. Zieger et al.

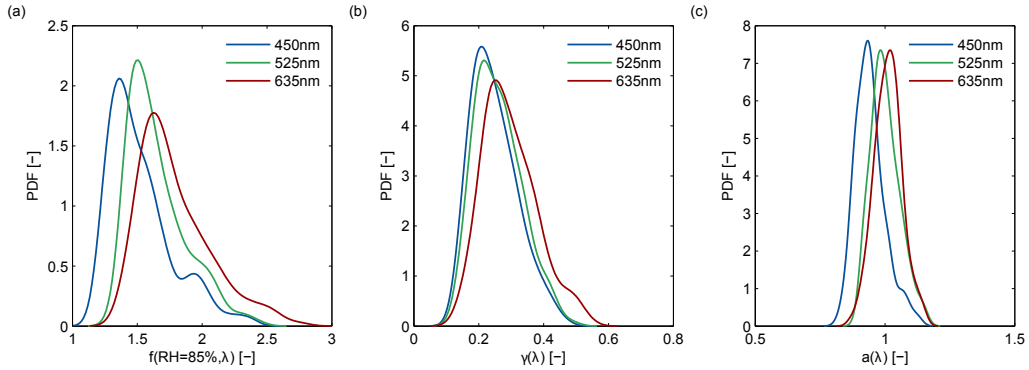

Figure 2. Probability density function (PDF) of **(a)** the measured $f(\mathrm{RH} = 85\,\%)$, **(b)** the fit-parameter γ (magnitude of $f(\mathrm{RH})$) and **(c)** and the fit parameter a (intercept). The different lines show the result for the three nephelometer wavelengths.

ACPD
15, 3327–3379, 2015

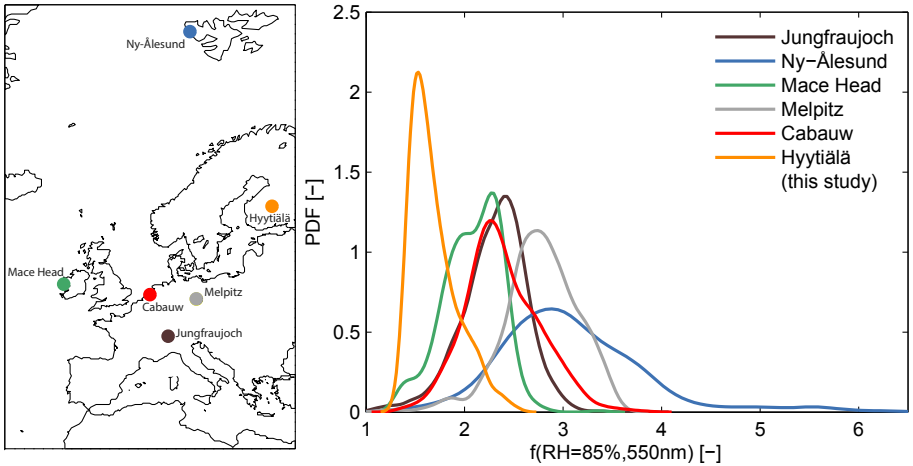

Figure 3. Probability density function (PDF) of the measured $f(\mathrm{RH} = 85\,\%,\ 550\,\mathrm{nm})$ at Hyytiälä (orange line) in comparison to results obtained at other European sites where the same instrument had been deployed (see legend; data taken from Zieger et al., 2013). The result for Hyytiälä was linearly interpolated to 550 nm wavelength. The left panel shows the location of the different sites.

ACPD
15, 3327–3379, 2015

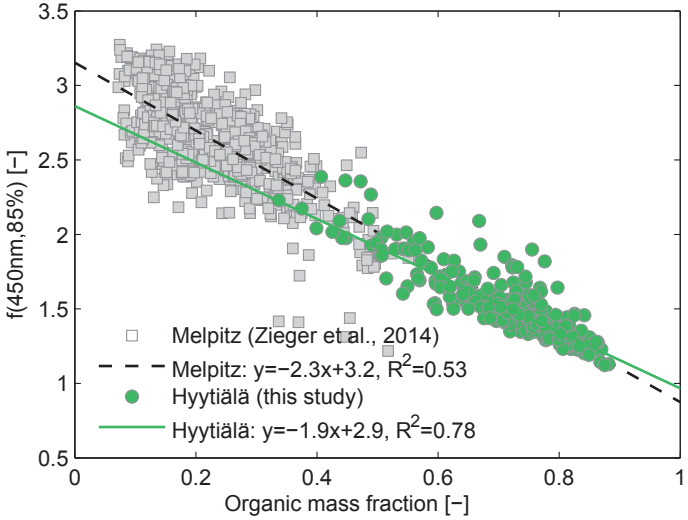

Figure 4. The scattering enhancement factor at RH = 85 % and λ = 450 nm vs. the organic mass fraction measured at Hyytiälä (green bullets) and Melpitz, Germany (grey squares). The solid and dashed line represent the corresponding linear least squares regressions.

ACPD
15, 3327–3379, 2015

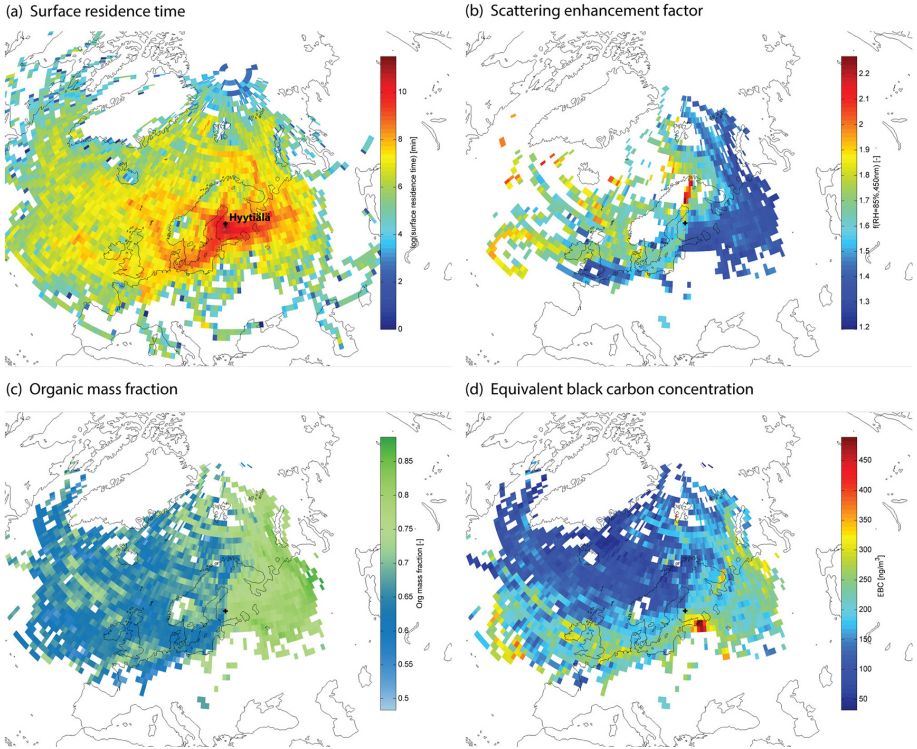

Figure 5. Results of the trajectory analysis (10 day backward calculations of air masses arriving at Hyytiälä, black cross, averaged on a 1° × 1° grid). **(a)** Total surface residence time, **(b)** scattering enhancement factor (at RH = 85 % and 450 nm), **(c)** organic mass fraction, **(d)** equivalent black carbon concentration.

ACPD
15, 3327–3379, 2015

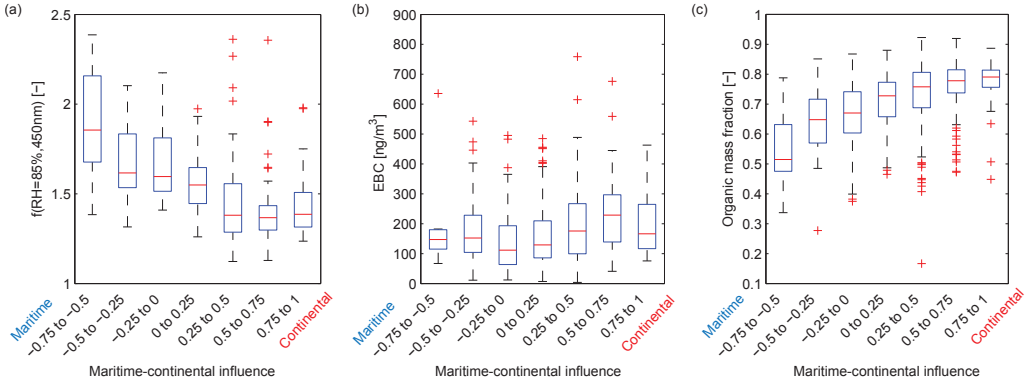

Figure 6. Box-plots of the **(a)** scattering enhancement $f(\mathrm{RH} = 85\,\%,\ 450\,\mathrm{nm})$, **(b)** equivalent black carbon concentration, and **(c)** organic mass fraction vs. the factor indicating the maritime and continental influence (see Eq. 4; as boundary: −1 would be a trajectory only traversing over oceans, +1 would be an air mass only traversing over land). The central red mark is the median, the edges of the box are the 25th and 75th percentiles, the error bars show the extent to the most extreme data points that are not considered as outliers, while the outliers are plotted individually (red crosses).

ACPD
15, 3327–3379, 2015

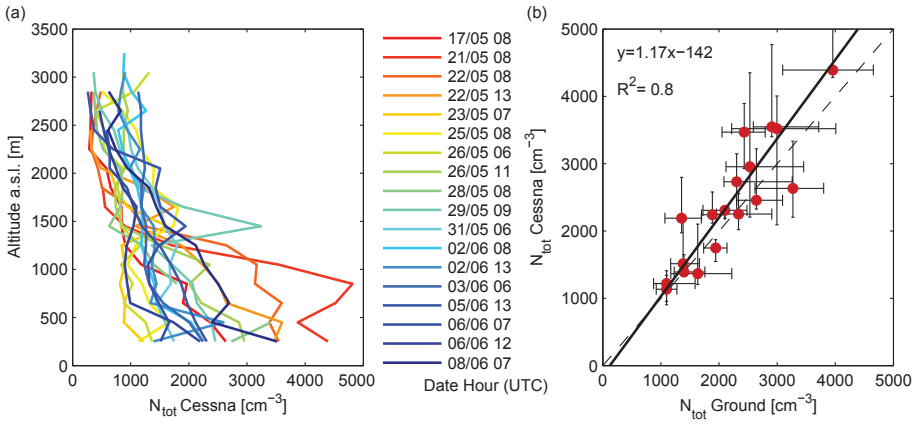

Figure 7. (a) Profiles of the total particle number concentration N_{tot} measured by the CPC on board the Cessna. Only the profiles with cloud free conditions are shown. Median values averaged every 200 m in altitude are shown. **(b)** Median of N_{tot} of the lowest flight level compared to the ground based measurement of the total CPC. The error bars denote the distance to the 25th and 75th percentile values. The solid line represents a linear least squares regression.

ACPD
15, 3327–3379, 2015

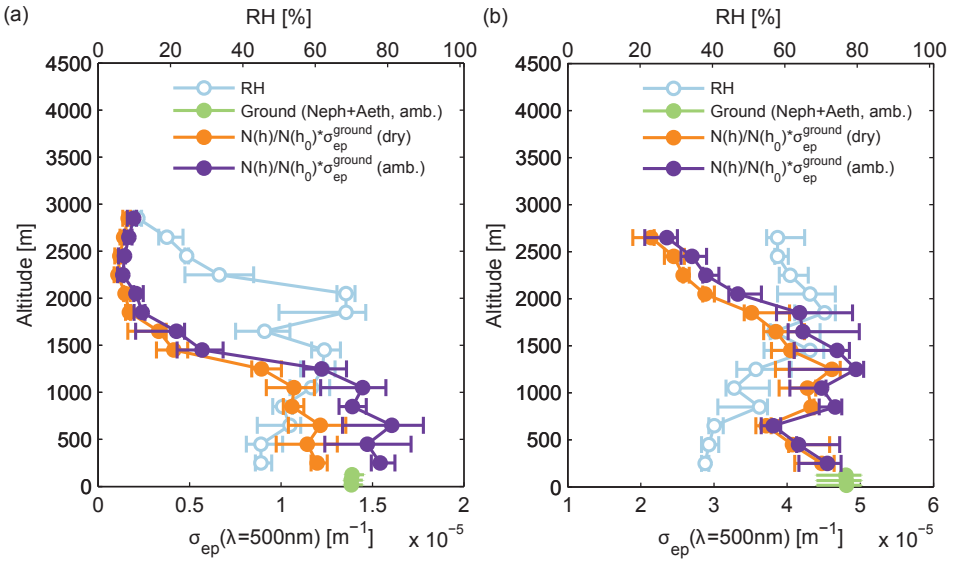

Figure 8. Example of the ground based in-situ measurements extrapolated to the atmospheric column. Particle light extinction coefficient (at λ = 500 nm) measured at the surface at ambient RH (along the tower at 17, 67 and 124 m; green bullets), surface extinction coefficient weighted with the relative changes in the total number concentration measured by the aircraft CPC (dry, orange points) and at ambient conditions (violet points) with the RH measured on board the aircraft (blue points, upper axis). The error bars denote the 25th and 75th percentile values. **(a)** Result for the 23 May 2013. **(b)** Result for the 2 June 2013.

ACPD
15, 3327–3379, 2015

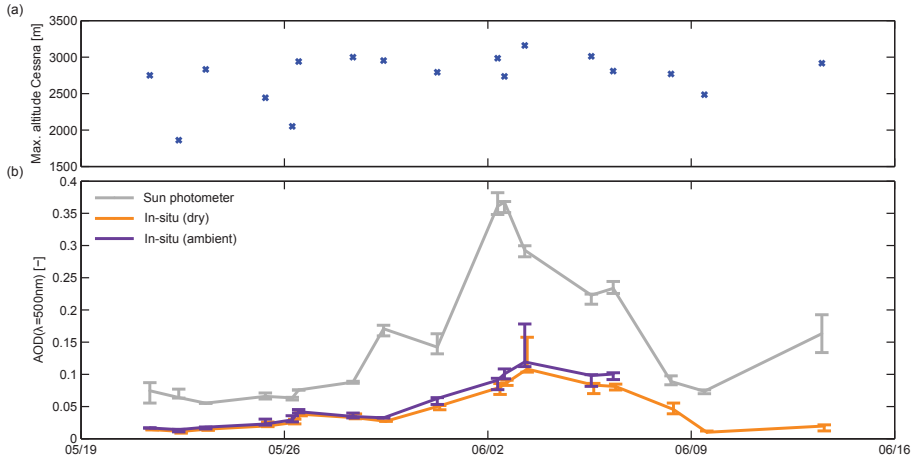

Figure 9. (a) Time series of the maximum altitude during the aircraft profiling. **(b)** Time series of the AOD at $\lambda = 500$ nm measured by the Sun photometer (grey curve), determined from the ground-based dry extinction coefficient and the airborne CPC as scaling factor (orange curve) and determined from the ground-based extinction coefficient at ambient conditions (violet curve). The error bars denote the distance to the 25th and 75th percentile values, while the center point gives the median value for each profile.

ACPD
15, 3327–3379, 2015

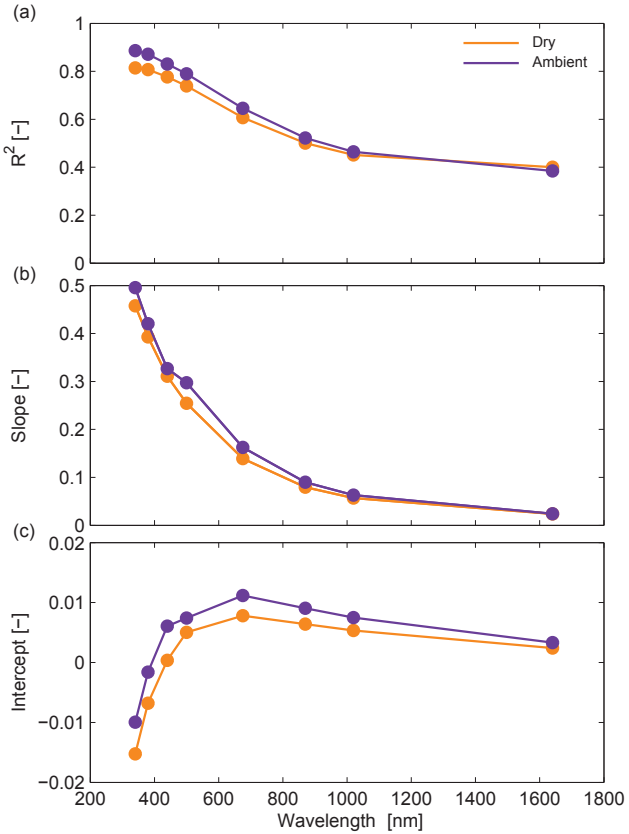

Figure 10. (a) Squared correlation coefficient, **(b)** intercept and **(c)** slope of all in-situ derived AOD values vs. the AERONET measurement for all available Sun photometer wavelengths. The colors refer to the dry and ambient profile calculations (see Fig. 8).

ACPD
15, 3327–3379, 2015

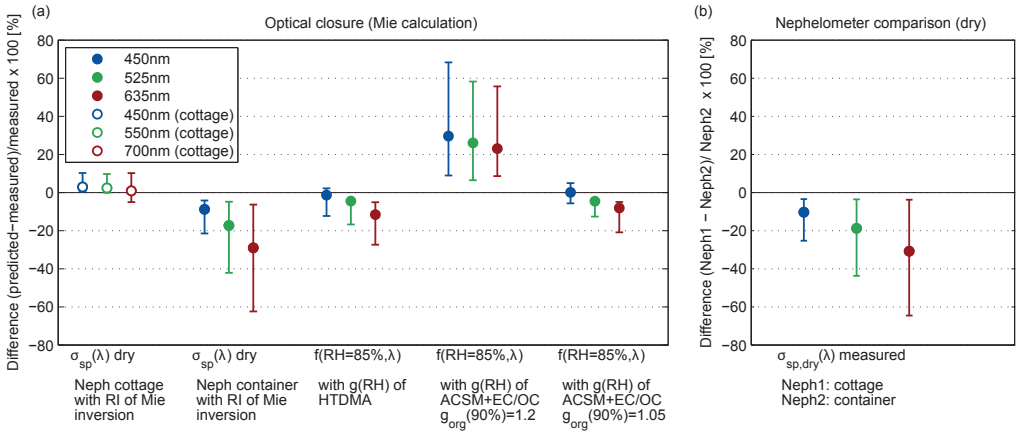

Figure 11. (a) Result of the optical closure study. Relative differences of the predicted to measured scattering coefficient (dry) and scattering enhancement factor (at RH = 85 %) for the different nephelometer wavelengths. The circle denotes the median value and the error bars the 25th and 75th percentile values. **(b)** Comparison of the dry nephelometer measurements ($\sigma_{sp,dry}$) between cottage (monitoring) and container (WetNeph). The values of the cottage nephelometer were interpolated using Eq. (6).

ACPD
15, 3327–3379, 2015

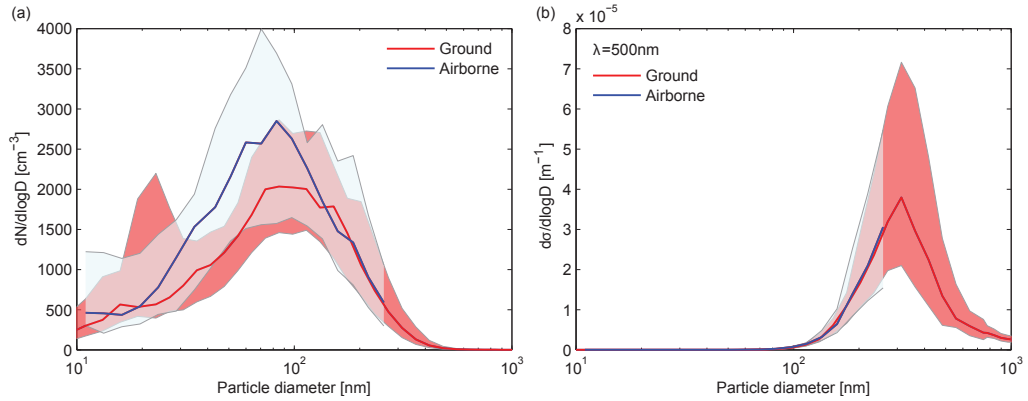

Figure 12. (a) Average particle number size distribution measured at ground and within the lowest flight level by the aircraft (200–400 m). **(b)** Aerosol scattering size distribution calculated using Mie theory for the wavelengths of 500 nm (RI = 1.51). The center lines show the median, while the corresponding shaded areas denote the 25th and 75th percentile values.

ACPD
15, 3327–3379, 2015

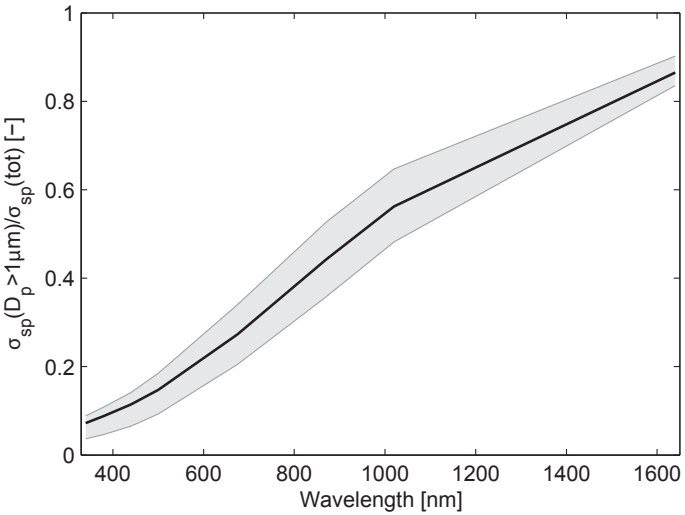

Figure 13. Coarse mode fraction of the particle light scattering coefficient vs. the Sun photometer wavelengths. The black center line shows the median value, while the shaded area denote the 25th and 75th percentile value range for the period with airborne measurements.

ACPD
15, 3327–3379, 2015

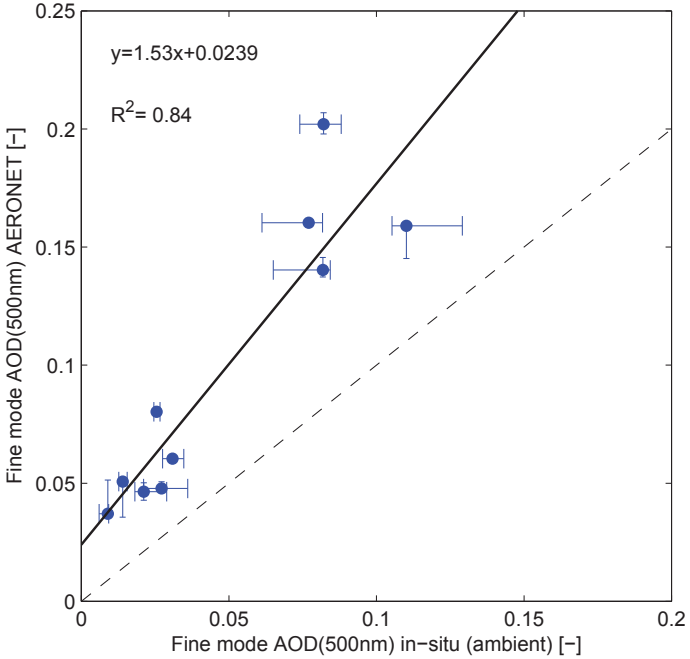

Figure 14. Aerosol optical depth (AOD) of fine mode particles derived from AERONET vs. the in-situ derived value using Mie theory and the measured size distribution (at 550 nm). The error bars denote the range of the 25th and 75th percentile values, while the center points mark the median value.

ACPD
15, 3327–3379, 2015

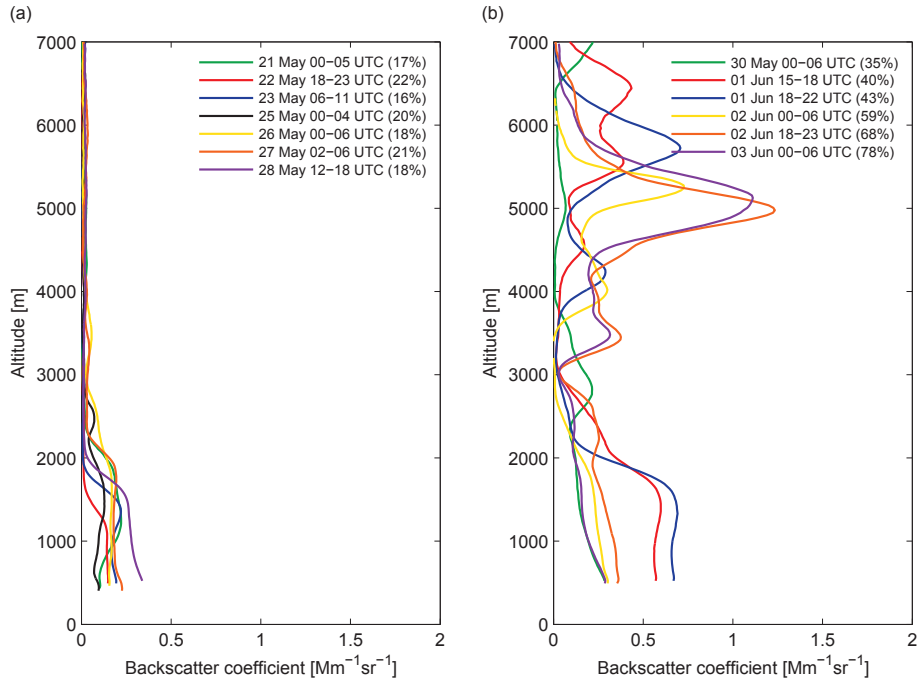

Figure 15. Aerosol backscatter coefficient profiles measured by the PollyXT lidar in Kuopio (200 km east-northeast of Hyytiälä) before **(a)** and during **(b)** the long-range transport period (λ = 1064 nm). The percental numbers in parenthesis denote the contribution of elevated layers above 3 km to the total AOD of the lidar profile.

ACPD
15, 3327–3379, 2015